

MASTER THESIS

# BIOPRINTABILITY OF DEX-TA/HA-TA HYDROGELS WITH HUMAN IPS CELLS FOR CARTILAGE TISSUE ENGINEERING

Laura Nauta

BIOMEDICAL ENGINEERING  
FACULTY OF SCIENCE AND TECHNOLOGY  
DEPARTMENT OF DEVELOPMENTAL BIOENGINEERING

## EXAMINATION COMMITTEE

Prof. dr. H.B.J. Karperien<sup>1</sup>  
Dr. S.K. Both<sup>1</sup>  
Dr. S. Simonsson<sup>2</sup>  
Dr. B. Zoetebier<sup>1</sup>  
Dr. ir. J. Rouwkema<sup>3</sup>

<sup>1</sup> Department of Developmental BioEngineering, Technical Medical Centre, University of Twente

<sup>2</sup> Institute of Biomedicine at Sahlgrenska Academy, Department of Clinical Chemistry and Transfusion Medicine, University of Gothenburg

<sup>3</sup> Vascularization Lab, Department of Biomechanical Engineering, Technical Medical Centre, University of Twente

12-09-19

UNIVERSITY OF TWENTE.

# ABSTRACT

Articular cartilage damage often leads to osteoarthritis, a major global cause of disability. Three-dimensional (3D) bioprinting holds large potential for cartilage tissue engineering, but there is a lack of suitable bioinks. In this study, the bioprintability of Dex-TA/HA-TA hydrogel with human induced pluripotent stem cells (iPSCs) was explored. Upregulation of ACAN expression in iPSCs was demonstrated for a variety of Dex-TA/HA-TA gel compositions. Enzymatic pre-crosslinking was successfully used to tune the viscosity of Dex-TA/HA-TA and create shear thinning bioinks. For the first time, printing and enzymatic post-crosslinking of such a bioink with iPSCs was demonstrated. However, sensitivity of the pre-crosslinking process yielded substantial variations in viscosity of the resulting bioink and was highly affected by the presence of iPSCs. In addition, pre-crosslinked bioinks show strong thixotropic behaviour including permanent viscosity loss, which could impair post-printing shape fidelity. In the future, a more robust 3D bioprinting platform for cartilage tissue engineering could be established by combining or replacing the enzymatic pre-crosslinking with another crosslinking mechanism, or increase the pre-printing viscosity using another approach.

# SAMENVATTING

Schade aan het gewrichtskraakbeen leidt vaak tot artrose, wereldwijd één van de grootste oorzaken van invaliditeit. Driedimensionaal bioprinten is een veelbelovende technologie voor het creëren van nieuw kraakbeenweefsel, maar er zijn nog onvoldoende geschikte materialen, zogenaamde bioinkten, hiervoor ontwikkeld. In dit onderzoek is de bioprintbaarheid van Dex-TA/HA-TA hydrogel met humane pluripotente stamcellen (iPSCs) onderzocht. Een verhoogde ACAN genexpressie werd aangetoond voor verscheidene gelsamenstellingen. Door middel van enzymatisch pre-crosslinking kon de viscositeit van Dex-TA/HA-TA worden aangepast en werden *shear thinning* bioinks verkregen. Het printen en vervolgens crosslinken van een dergelijke bioinkt met iPSCs werd voor het eerst gedemonstreerd. Het sensitieve pre-crosslinkingproces leidde echter tot grote variaties in viscositeit en werd aanzienlijk beïnvloed door de aanwezigheid van cellen. Daarnaast vertoonden de bioinkten sterk thixotroop gedrag en permanente viscositeitsreductie, wat de vormvastheid na het printen negatief beïnvloedt. Een verbeterd 3D-printplatform voor kraakbeenweefsel zou in de toekomst bereikt kunnen worden door het enzymatische pre-crosslinkmechanisme te combineren met of vervangen door een ander crosslinkmechanisme, of de viscositeit van Dex/HA op een andere manier te verhogen.

# TABLE OF CONTENTS

<b>ABSTRACT / SAMENVATTING</b>	<b>2</b>
<b>List of symbols and abbreviations</b>	<b>4</b>
<b>1 Introduction</b>	<b>5</b>
1.1 Articular cartilage damage .....	5
1.2 Three-dimensional bioprinting for cartilage repair.....	6
1.3 Bioprinting potential of Dex/HA with induced pluripotent stem cells .....	9
1.4 Enzymatic crosslinking mechanism: implications for bioprinting.....	10
1.5 Thesis outline .....	12
<b>2 Materials &amp; Methods</b>	<b>14</b>
2.1 Hydrogel preparation.....	14
2.2 Rheological analysis .....	15
2.3 Bioprinting .....	16
2.4 Cell culture, encapsulation and chondrogenesis.....	18
2.5 Evaluation of cellular activity and chondrogenesis.....	19
2.6 Compatibility of pre-crosslinked Dex/HA and iPSCs for bioprinting .....	19
<b>3 Results</b>	<b>20</b>
3.1 Creation of a viscous bioinks by enzymatic pre-crosslinking of Dex/HA.....	20
3.2 Rheological properties of pre-crosslinked Dex/HA.....	22
3.4 Printability of pre-crosslinked Dex/HA.....	25
3.4 Effect of Dex/HA gel composition on iPSC metabolism and ACAN expression.....	28
3.5 Combining pre-crosslinked Dex/HA bioink with iPSCs .....	32
<b>4 Discussion</b>	<b>34</b>
4.1 Enzymatic pre- and post-crosslinking of Dex/HA.....	34
4.2 Rheological properties of pre-crosslinked Dex/HA.....	35
4.3 Printability.....	36
4.4 Dex/HA as a carrier for iPSC chondrogenesis and bioprinting .....	37
4.5 Metabolic activity of iPSCs in Dex/HA.....	38
4.6 Bioprinting of iPSC-laden Dex/HA.....	39
4.7 Recommendations and future outlook .....	40
<b>5 Conclusions</b>	<b>42</b>
<b>Acknowledgements</b>	<b>43</b>
<b>REFERENCES</b>	<b>44</b>
<b>Appendix 1: Supplementary data</b>	<b>49</b>
<b>Appendix 2: Printability assessment g-code</b>	<b>53</b>

# LIST OF SYMBOLS AND ABBREVIATIONS

$\dot{\gamma}$	shear rate
$\eta$	apparent viscosity
$\tau$	shear stress
$\tau_0$	yield stress
$G'$	storage modulus
$G''$	loss modulus
$m$	flow consistency index
$n^*$	flow behaviour index
3D	three-dimensional
3ITT	three interval thixotropy test
ACAN	aggrecan
ACI	autologous chondrocyte implantation
CAD	computer-aided design
CTE	cartilage tissue engineering
Da	dalton
ddH <sub>2</sub> O	double distilled water
Dex(-TA)	(tyramine-substituted) dextran
DG	double gap
DMEM	Dulbecco's modified Eagle's medium
DPBS	Dulbecco's phosphate buffered saline
DS	degree of substitution
G	Gauge
GFP	green fluorescent protein
H&E	haematoxylin and eosin
H <sub>2</sub> O <sub>2</sub>	hydrogen peroxide
HA(-TA)	(tyramine-substituted) hyaluronic acid
HRP	horseradish peroxidase
Hz	hertz
iPSC	induced pluripotent stem cell
MACI	matrix-induced autologous chondrocyte implantation
mRNA	messenger ribonucleic acid
MSC	mesenchymal stem cell
MW	molecular weight
NFC	nanofibrillated cellulose
OA	osteoarthritis
Pa	pascal
PBS	phosphate buffered saline
PCL	polycaprolactone
PP	parallel plates
TA	tyramine
TGF- $\beta$	transforming growth factor beta
U	active unit
UV	ultraviolet

# 1 INTRODUCTION

## 1.1 Articular cartilage damage

Joint trauma, for instance resulting from an accident or sports injury, often leads to damage of the articular cartilage. This severely increases the risk to develop osteoarthritis (OA) [1, 2], a degenerative disease of the joints characterized by articular cartilage degeneration, formation of osteophytes on the subchondral bone and joint inflammation. As a result, patients experience joint pain, stiffness and functional limitations, leading to a decreased quality of life [3-5]. To date, no disease-modifying treatment for OA exists. Instead, standard treatments primarily include pain management, sometimes combined with lifestyle adaptations to delay the progression of the disease [6]. Total joint replacement is currently the only end-stage treatment. The need for strategies to prevent the onset of posttraumatic OA is high, since it often concerns young and active patients, for which the limited durability and functionality of a total joint replacement are not acceptable [7]. Also in primary (non-posttraumatic) OA, it has been shown that cartilage defects lead to further progression of the disease [8-10].

An explanation for the devastating consequences of cartilage defects can be found in the composition and properties of the tissue. Articular cartilage is a layer of hyaline cartilage covering articulating bone surfaces. The function of this tissue is to enable smooth, frictionless joint movement and to provide load distribution onto the subchondral bone. It is characterized by its dense, highly hydrated extracellular matrix, low cell density and absence of vasculature. Structurally, four different zones between the joint surface and the subchondral bone can be distinguished that provide different functions such as surface lubrication (superficial zone) and smooth integration with the subchondral bone (calcified zone). Collagen type II, the most abundant structural matrix component, provides resistance against tensile and shear stresses. Collagens are intertwined with a network of proteoglycans and hyaluronic acid. The negatively charged proteoglycans, of which aggrecan is the most abundant type, attract large quantities of water into the cartilage. High retention of fluid allows the tissue to withstand compression forces. Matrix production and maintenance is provided by chondrocytes, the only cell type residing in articular cartilage. The small quantity and low proliferative potential of chondrocytes, along with the high cartilage matrix density and absence of vasculature, limits migration of chondrocytes into a defect site. As a result, cartilage possesses a poor intrinsic repair capacity. Prolonged damage disrupts tissue homeostasis, leading to the onset of OA. Thus, repairing cartilage defects in an early stage appears to be essential to prevent the onset or progression of OA.

The first type of therapy attempting regenerative cartilage repair is microfracture, clinically available since the early 1990s [11]. This therapy is based on bone marrow stimulation: cells from the underlying bone marrow are allowed to migrate into the defect site, where they proliferate and produce matrix. However, the resulting tissue is fibrous, associated with inferior mechanical properties compared to hyaline cartilage, and therefore has a durability of only several years [12]. First proposed in 1994, autologous chondrocyte implantation (ACI) has been added to the clinically available treatments for cartilage defects [13]. In a first surgery, cartilage is harvested from a relatively non-loaded area of the joint. Chondrocytes are isolated and expanded *in vitro*, after which they are transplanted into the defect site and covered with a periosteal flap or collagen membrane. This treatment yields more hyaline-like neocartilage [14] and higher durability [15], but is very costly due to the need for two surgical interventions, extended cell culturing (typically around 6 weeks) and prolonged rehabilitation [16-18]. As a result of its low cost-effectiveness, ACI is often not covered by health insurers. Other drawbacks of this procedure are donor site morbidity and de-differentiation of chondrocytes *in vitro*. To prevent the latter, chondrocytes have been cultured on a scaffold before transplantation, a procedure called matrix-induced ACI (MACI). Several materials are in clinical use for this procedure with promising results [19].

With respect to cartilage repair, MACI is the first approach based on tissue engineering: the field which aims to generate functional tissue using a combination of scaffolds, cells and/or bioactive signals. Many cartilage tissue engineering (CTE) strategies are under investigation; not only to improve current treatments, but also to develop innovative, cost-effective treatments and create *in vitro* tissue models for studying pathology, tissue development and drug responses.

## **1.2 Three-dimensional bioprinting for cartilage repair**

An appealing approach in CTE is three-dimensional (3D) bioprinting, an additive manufacturing technique that allows superior spatial resolution and control over the distribution of multiple materials and cell types. 3D bioprinting allows rapid prototyping of complex structures that are created in a layer-by-layer fashion, based on computer-aided design (CAD). It is possible to translate clinical imaging data into a print design, allowing the generation of patient-specific constructs. The three main bioprinting techniques are inkjet, extrusion-based and laser-assisted printing, each with their own advantages and limitations. However, extrusion printing is most widely used because of the relatively low costs, ease of operation and flexibility to a wide range of viscosities and cell densities.

Cartilage has been a main candidate for 3D bioprinting since the technology has emerged, considering the urgent clinical need on one hand, and the tissue's relative simplicity, with only one cell type and absence of vasculature, on the other hand. Using 3D bioprinting and patients'

imaging data, constructs could be created that exactly match an individual cartilage defect. In addition, this manner of manufacturing allows the recapitulation of the different zones in articular cartilage, which has the potential to enhance mechanical properties and, in case of full osteochondral defects, integration with the underlying bone.

While bioprinting techniques are rapidly advancing, it remains a challenge to develop appropriate printing materials, so-called bioinks. Mostly, this challenge emerges from the unfortunate fact that biological and printing requirements often compromise each other. First of all, the bioink has to meet traditional tissue engineering requirements, such as providing a suitable 3D environment to direct cell fate, proliferation and tissue formation, as well as to enable immunoprotection, entrapment and homogeneous distribution of encapsulated cells. Ideally, a CTE material has a degradation profile that matches the rate of neocartilage formation. Second, the bioink has to meet printability requirements: flow during extrusion, prevent cells from high shear stress during printing and (re)gain shape stability rapidly after extrusion. Finally, the resulting construct has to possess appropriate mechanical properties.

It is worth mentioning that the development of bioinks is additionally hampered by the lack of consensus on the definition of printability and standardized methods to assess printability; as well as by poor knowledge on material properties that can predict printability. A few groups have dedicated studies to this topic and have shown the significance of viscosity, yield stress and storage modulus recovery [20-27]. In addition, storage and loss modulus and loss tangent [20] as well as viscosity recovery after stress [25] have been suggested as printability predictors.

Several materials that are known to support or promote neocartilage formation have been investigated for their 3D bioprinting potential. In general, hydrogels are the materials of choice since, like the extracellular matrix, they consist of a highly hydrated polymer network. Alginate has gained most attention, since it is known to support chondrogenesis and offers easy and rapid ionic crosslinking. Daly et al. compared different bioinks loaded with mesenchymal stem cells (MSCs) and found alginate to be superior in yielding hyaline-like cartilage tissue formation *in vitro* compared to agarose, methacrylated gelatin (GelMA) and methacrylated polyethylene glycol (PEGMA) [28]. However, printed alginate structures had poor shape fidelity and mechanical strength. Therefore, polycaprolactone (PCL) filaments were incorporated, which enhanced the printability and mechanical properties. Following the same approach, hybrid constructs of up to 1.8 mm high were printed using PCL and chondrocyte-laden alginate, in which hyaline-like matrix production was demonstrated *in vitro* [29], as well as *in vivo* [30].

In a recent study by Yang et al., addition of collagen type I to alginate was shown to improve mechanical strength [31]. In small 3D printed constructs, increased chondrocyte adhesion,

proliferation and matrix protein expression was observed. Markstedt et al. combined alginate with nanofibrillated cellulose (NFC), leading to increased viscosity and shear thinning [32]. This bioink allowed creation of large 3D constructs with good chondrocyte viability. In more recent work with the same bioink, chondrogenesis of induced pluripotent stem cells was demonstrated in constructs of 1.2 mm in height [33].

Costantini et al. combined alginate with different photocurable polymers [34]. MSC-laden bioinks were successfully printed using coaxially extruded calcium chloride for instantaneous alginate crosslinking and UV light for secondary crosslinking. Constructs up to 5 mm high, with different geometries, were successfully printed with 100  $\mu\text{m}$  layer thickness and inter-fibre distance of 300  $\mu\text{m}$ . In a recent follow-up, the group expanded their printing system with a microfluidic printhead for multi-material printing, which was utilized to recapitulate the zonal structure of cartilage [35]. With two distinct bioinks, hyaline and calcified cartilage were mimicked. The latter bioink indeed presented upregulation of hypertrophic factors compared to the former. Biphasic constructs were bioprinted and after one month *in vitro*, implanted into osteochondral defects *in vivo*. Histological analysis after twelve weeks showed superior cartilage repair compared to no-treatment control.

As a natural cartilage component with shear thinning ability, hyaluronic acid (HA) holds large potential for 3D printing of cartilage-like tissue. However, also HA requires mechanical reinforcement. It can be tricky to tune the properties of HA-based hydrogels, since molecular weight and concentration are known to have a significant influence on its functionality [36]. This was clearly demonstrated by Mouser et al, who found that addition of 0.25% - 0.5% w/w methacrylated HA (HAMA; 120 kDa) to their bioink resulted in hyaline-like matrix production, while higher HAMA concentrations (1%) resulted in fibrocartilage formation [37]. This might explain why the addition of HA was not very successful for hyaline cartilage formation in some of the aforementioned studies: in the work of Costantini et al, addition of HAMA (200 kDa, 0.5% w/w) to their ink led to hypertrophy [34, 35], while iPSCs printed in alginate with tyramine-substituted HA (~1MDa), led away from pluripotency in an early phase [33].

Although these studies show exciting results, the hydrogel systems have substantial drawbacks. In cases with good printability, chondrogenic potential of the bioink was often inferior, although researchers try to improve this by including TGF- $\beta$ , other growth factors or extracellular matrix powder in the bioink [30, 38, 39]. Compressive moduli matching the native cartilage have been achieved only with the use of PCL, but this material lacks bioactivity, needs to be extruded at 60°C and has a slow degradation rate, which hampers replacement by neocartilage *in vivo*. An initial construct does not need to be as strong as native tissue, as long as the material is gradually replaced by neocartilage. Therefore, also cellulose and other viscosity-enhancing agents that have a slow degradation rate, might hamper cartilage regeneration. The work of

Costantini et al. emphasized the importance of crosslinking mechanisms to enhance bioprinting systems. However, UV crosslinking as used in their work and that of many others, compromises cell viability and function. The combination of highly chondrogenic materials and appropriate, mild crosslinking mechanisms holds a lot of potential.

### **1.3 Bioprinting potential of Dex/HA with induced pluripotent stem cells**

The Developmental BioEngineering group at the University of Twente has developed a tunable hydrogel system based on the enzymatic crosslinking of tyramine-functionalized polysaccharides under mild conditions. Designed to obtain an injectable, *in situ* gelating hydrogel for cartilage repair, it has been shown that this crosslinking mechanism allows tuning of both crosslinking speed and mechanical strength within a suitable range [40]. In addition, excellent tissue-implant integration can be achieved through covalent bonds with tyrosine-containing proteins in the native cartilage [41]. In particular, a hydrogel composed of tyramine-substituted dextran (Dex-TA) and hyaluronic acid (HA-TA) in 50/50 ratio has proven to be very effective in attracting cells and promoting chondrogenesis [42]. Spin-off company Hy2Care is currently commercializing this minimally invasive and cell-free injectable hydrogel technology for cartilage repair. After promising animal studies, the first clinical trials are now expected to start within 1.5 years.

The tunability of the crosslinking process and bioactivity of the resulting hydrogels offer many possibilities. Several applications are being investigated by the Developmental BioEngineering group, such as microfluidics-based cell encapsulation with tunable matrix stiffness and introduction of functional vascularization in the hydrogel [43-46]. It would be very interesting to see if the tunable system also enables the creation of a printable bioink. In combination with the material's outstanding chondrogenic capacity, this could potentially outperform existing cartilage bioprinting platforms.

The Dex-TA/HA-TA (50/50) hydrogel, in short Dex/HA, has been extensively used in combination with mesenchymal stem cells (MSCs) and demonstrated high viability, metabolic activity and differentiation potential [44, 47]. The use of this cell type for cartilage repair holds a lot of advantages compared to chondrocytes, such as increased accessibility and proliferative potential. However, with respect to clinical translation, MSCs also present a few important limitations. MSC populations are heterogeneous in terms of chondrogenic differentiation potential [48] and have a tendency towards hypertrophy, leading to ossification *in vivo* [49, 50]. In addition, the proliferation potential of MSCs decreases with age [51, 52]. Therefore, in the field of tissue engineering interest has grown for the use of induced pluripotent stem cells (iPSCs), introduced by Yamanaka et al. in 2007 [53]. iPSCs present pluripotency and infinite self-renewal potential, without the ethical concerns that are related to embryonic stem cells.

For various applications, autologous iPSCs are considered to be the ideal cell source. However, CTE has less restrictions with respect to cell origin, since articular cartilage has been suggested to be immune-privileged due to the tissue's avascularity and dense matrix [54, 55]. Instead of preparing iPSCs for each individual patient, which is costly, time-consuming and expected to yield large variability in clinical outcome, a universal, allogeneic iPS cell line could be established that is selected for its efficiency in promoting neocartilage formation. Due to the infinite self-renewal of pluripotent cells, this would provide an efficient off-the-shelf therapy with robust clinical outcome. Although currently the majority of iPS cell lines is fibroblast-derived, it has been suggested that iPSCs maintain epigenetic memory and therefore present a preference for the differentiation pathway towards their cell type of origin [56-58]. Therefore, the Molecular Cell Biology and Regenerative Medicine group at the Sahlgrenska Academy in Gothenburg reprogrammed surplus ACI donor chondrocytes using a non-integrating mRNA-based reprogramming protocol [59]. The resulting iPSCs show high chondrogenic potential, especially one particular line labelled 'A2B'. This demonstrates how selection of donor or even donor cell subpopulation can be used to improve therapy efficacy. Similarly, iPS cell lines from OA patients can be selected for *in vitro* disease modelling and drug testing.

From 2011 on, several groups have reported on the optimization of iPSC chondrogenesis protocols [60-70]. Next to defined chondrogenic factors, such as members of the TGF- $\beta$  superfamily, the importance of 3D culturing has been pointed out. The A2B line has shown successful *in vitro* chondrogenesis in a pellet culture, but the use of a hydrogel-based carrier might provide a better platform for clinical applications, as well as provide additional cues enhancing neocartilage formation. In the quest for suitable carrier materials, a collaboration was established with the department of Developmental BioEngineering at the University of Twente. Upregulation of chondrogenic markers and enhanced matrix secretion of iPSCs in Dex/HA *in vitro* have been demonstrated [71]. In the same study, Dex/HA gels containing pre-differentiated iPSCs or iPSCs co-cultured with irradiated chondrocytes, were subcutaneously implanted in mice. Histological assessment after four weeks showed a much more hyaline-like appearance of the newly formed tissue, compared to the commercial Hyaff membrane seeded with chondrocytes. Since the feasibility of 3D bioprinting cartilage constructs with this cell line has already been demonstrated [33], bioprinting these iPSCs in Dex/HA seems very promising.

#### **1.4 Enzymatic crosslinking mechanism: implications for bioprinting**

As mentioned, the Dex/HA hydrogel system has been designed for injection and is based on enzyme-catalysed oxidation of phenol groups. More specifically, the enzyme horseradish peroxidase (HRP) reacts with a hydrogen peroxide ( $H_2O_2$ ) molecule (**Figure 1**). The enzyme returns to its original state via two steps, each step involving the oxidation of a tyramine (TA)

group that is connected to a polysaccharide backbone. Subsequently, two TA radicals can couple with each other to form a covalent crosslink. To summarize, each catalytic cycle leads to the consumption of one  $\text{H}_2\text{O}_2$  molecule and formation of two TA radicals, while HRP is recycled.

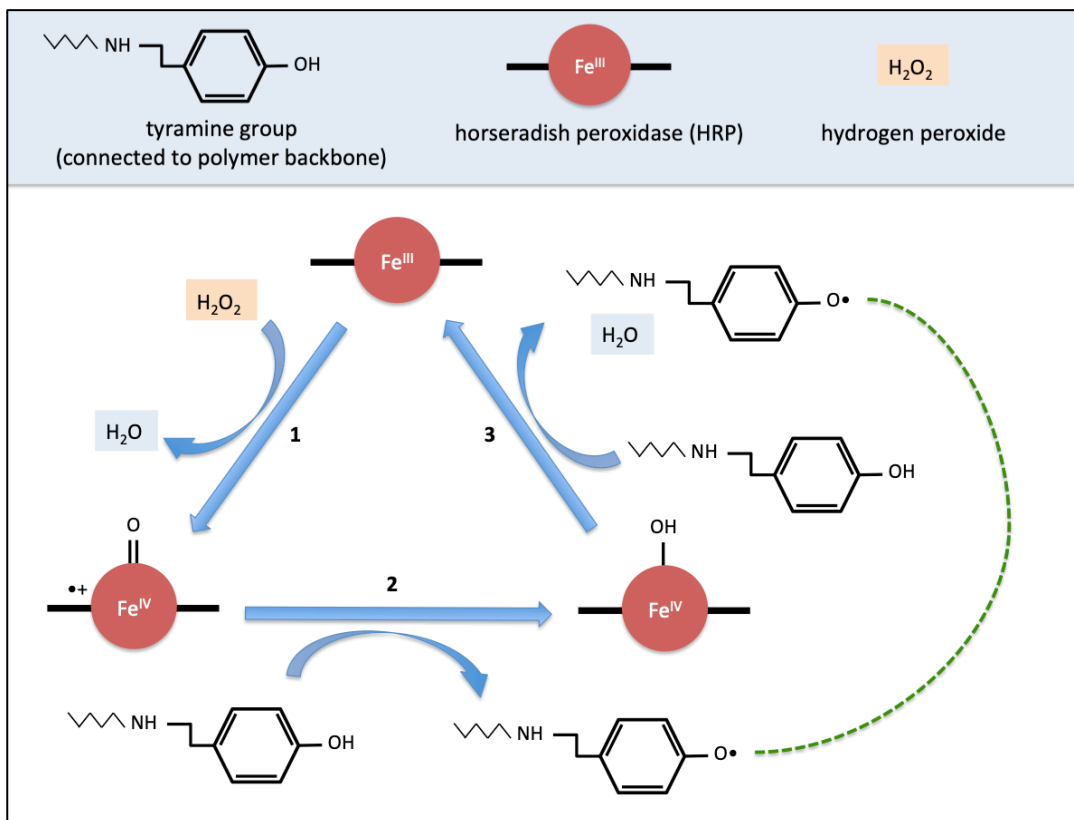


**Figure 1:** HRP/ $\text{H}_2\text{O}_2$  mediated crosslinking mechanism of tyramine-substituted polymers. 1) The heme group of HRP is oxidized under reduction of  $\text{H}_2\text{O}_2$  to  $\text{H}_2\text{O}$ . 2) The now reactive HRP compound subtracts a hydrogen molecule from tyramine, resulting in a tyramine radical. 3) HRP-bound hydroxyl group forms a  $\text{H}_2\text{O}$  molecule together with a hydrogen molecule from tyramine, creating a second tyramine radical. HRP has now returned to its initial state and the enzymatic cycle can be repeated.

The degree of crosslinking, dictating the mechanical strength of the hydrogel, is determined by the  $\text{H}_2\text{O}_2/\text{TA}$  molar ratio, which is theoretically saturated at 0.5  $\text{H}_2\text{O}_2/\text{TA}$ . Because excess  $\text{H}_2\text{O}_2$  can both inhibit the crosslinking process, as well as be detrimental to cell viability, an optimized  $\text{H}_2\text{O}_2/\text{TA}$  ratio of  $\sim 0.2$  has been established, yielding storage moduli of around 10 kPa for Dex/HA with 10% w/v polymer concentration. The number of catalytic cycles that can occur simultaneously, and therefore the crosslinking rate, is controlled by the HRP concentration. The gelation time can be tuned within the order of seconds to minutes, using between 1 – 4 active units (U) HRP per mL.

After combining the polymers, HRP and H<sub>2</sub>O<sub>2</sub>, this delayed gelation process provides enough time to inject the material while it is still fluid and let it fill an entire cartilage defect, even when irregularly shaped. Subsequently, within minutes a rather immediate switch from fluid to solid gel occurs. At the same time, the hydrogel covalently adheres to adjacent cartilage tissue.

For bioprinting, however, the requirements of a hydrogel/crosslinking system are different. When printing a liquid material such as non-crosslinked Dex/HA, immediate crosslinking upon extrusion is required for the extruded material to maintain shape. The HRP/H<sub>2</sub>O<sub>2</sub> crosslinking system, which is in the order of seconds at fastest, is too slow. In general, there are two approaches to overcome this problem: either to accelerate the crosslinking, or adjust the properties of the material before extrusion. For the first approach, another crosslinking system must be incorporated. To this end, ionic crosslinking of sodium alginate is a good candidate, because it presents immediate crosslinking. In addition, alginate can be washed out of the construct, thereby avoiding its interference in the final gel composition.

For the second approach, a variety of options exists to adjust the rheological properties of the gel precursor. Increasing the polymer concentration will lead to increased viscosity, but further delays crosslinking [42] and might limit nutrient diffusion, cell migration and proliferation. Another option is the addition of a high molecular weight (MW) polymer, although this might also affect the cellular response. An elegant alternative solution, which has become the main focus of this thesis, could be offered by pre-crosslinking the gel precursor using the HRP/H<sub>2</sub>O<sub>2</sub> system, followed by additional crosslinking after printing. Pre- and post-crosslinking using the same modality has been reported for the ionic crosslinking of sodium alginate [72], but not yet for enzymatic crosslinking. However, Petta et al. have succeeded to obtain a printable bioink by pre-crosslinking tyramine-functionalized HA (280 kDa) in the presence of H<sub>2</sub>O<sub>2</sub> and HRP [73].

## **1.5 Thesis outline**

The aim of this project was to investigate the feasibility of 3D bioprinting of Dex/HA, in particular combined with human iPSCs. Part of this research was executed at the Molecular Cell Biology group in Gothenburg and focused on 1) optimizing Dex/HA as a carrier material for iPSCs and 2) establishing the proof of concept for Dex/HA bioprinting based on enzymatic pre- and post-printing crosslinking. At the department of Developmental BioEngineering in Twente, extensive rheological analysis was performed, as well as assessment of printability.

In this thesis, it will first be demonstrated how viscous pre-crosslinked Dex/HA solutions were obtained, displaying bioink-like viscosity and shear thinning. Next, the rheological properties of pre-crosslinked Dex/HA will be discussed and will be related to its printability. In addition to a printability assessment, which focused on (two-dimensional) filament formation, the feasibility of

three-dimensional printing and post-crosslinking was investigated. The effects of Dex/HA concentration and solvent on iPSC viability and chondrogenesis were studied with the aim to optimize Dex/HA as a carrier material for iPSCs. Finally, the implications of loading pre-crosslinked Dex/HA with iPSCs on the viscosity, cell sedimentation and printing were reported.

## 2 MATERIALS & METHODS

### 2.1 Hydrogel preparation

#### *Polymer synthesis and characterization*

Tyramine-substituted polymers were synthesized by staff members of the Developmental BioEngineering group. Dextran (40 kDa) was functionalized either as previously described [74], referred to as the old method (O), or following a slightly altered new method (N), which has not been published yet. Hyaluronic acid (25 kDa) was functionalized with tyramine as previously described [74]. The degree of substitution (DS) determined using  $^1\text{H}$  NMR was 10 for HA-TA (tyramine groups per 100 disaccharide units) and ranged from 11 to 16 for Dex-TA batches (tyramine groups per 100 monosaccharide units). An overview of polymer batches is attached in the supplementary data (**Table S1**).

#### *Hydrogel formation*

Tyramine-substituted polymers were dissolved at 12.5 % (w/v) at least one day before further use. Solutions of Dex-TA, HA-TA (always in 50/50 ratio) and horseradish peroxidase (HRP; Sigma-Aldrich) were mixed at the day before crosslinking and stored protected from light. This mixture will be referred to as the gel precursor. On the day of gel formation or crosslinking, a  $\text{H}_2\text{O}_2$  solution was prepared from 30 wt % stock solution (Sigma-Aldrich) and added to the gel precursor in 1:9 ratio, immediately followed by 5 seconds of vortexing to achieve homogeneous crosslinking. Both the gel precursor and  $\text{H}_2\text{O}_2$  solution were kept on ice before mixing, in order to delay and control the gelation. End concentrations of polymer, HRP and  $\text{H}_2\text{O}_2$  ranged between 2.5 – 10% weight by volume (w/v), 1 – 4 U/mL and 0.0015 – 0.033% w/v, respectively. The gelation times of different hydrogel compositions were determined using the vial tilting method and defined as the time from adding  $\text{H}_2\text{O}_2$  to the precursor until no longer any flow could be observed in the sample (volume: 50 or 100  $\mu\text{L}$ ).

For most experiments, Dex-TA and HA-TA were dissolved in PBS (Lonza) or DPBS (Gibco™). In addition, DMEM (low glucose, sodium pyruvate; Gibco™ Cat No. 31885-023), 70  $\mu\text{g}/\text{mL}$  Matrigel® (Corning®, Cat No. 354230) and double distilled water ( $\text{ddH}_2\text{O}$ ) were used as solvents for polymer solutions. HRP and  $\text{H}_2\text{O}_2$  were always dissolved or diluted, respectively, in (D)PBS.

In this report, Dex/HA is used as the short notation for Dex-TA/HA-TA, where deemed necessary preceded by the polymer concentration and/or followed by  $\text{H}_2\text{O}_2/\text{TA}$  molar ratio, i.e. 5% Dex/HA 0.040 is Dex-TA/HA-TA with 5% polymer content, crosslinked using 0.040 mol  $\text{H}_2\text{O}_2$  per mol TA. Polymer and  $\text{H}_2\text{O}_2$  concentrations always express the weight by volume percentage. The active

unit (U) used to quantify HRP is defined as the amount of HRP that catalyses the production of 1 mg of purpurogallin from pyrogallol in 20 seconds at 20°C and pH 6.0. Furthermore, the term 'gelation' will only be used for crosslinking that results in a solid, non-flowing gel.

## 2.2 Rheological analysis

Rheological experiments were performed with a MCR 301 rheometer (Anton-Paar) with Peltier temperature control (C-PTD200) using parallel plates (PP;  $\varnothing$  25 mm, 0°) or double gap configuration (DG26.7). In both configurations, measurements were performed at 20°C, unless indicated otherwise, although temperature is controlled to a higher degree in double gap (DG) configuration. Hydrogel samples were prepared just in advance, so that the sample could be applied onto the ground plate or into the cup before crosslinking had completed. After applying the sample, the upper plate or spindle was lowered and the sample was allowed to crosslink for at least 60s before initiating the measurement. In PP configuration, the measurement was started directly afterwards to prevent the sample from drying out. In DG configuration, where the sample is largely protected from drying out, measurement was started after establishment of thermal equilibrium (target temperature  $\pm 0.1^\circ\text{C}$ ).

Preliminary viscosity measurements were performed in PP configuration ( $\varnothing$  25 mm, 0.8 mm gap), which is less reliable than DG configuration, but required a 7-fold smaller quantity of material. Shear viscosity or apparent viscosity  $\eta$ , defined as the shear stress  $\tau$  divided by the shear rate  $\dot{\gamma}$ , was determined using a logarithmic shear rate sweep from 0.01/s to 1000/s. The viscosity of Dex/HA with 5% polymer concentration and various  $\text{H}_2\text{O}_2/\text{TA}$  ratios was additionally determined in double gap configuration by a shear rate sweep from 0.01/s to 10,000/s. As an indication of the degree of shear thinning, flow behaviour index  $n^*$  was calculated using the Power Law relationship between shear rate and shear stress:

$$\tau = m * \dot{\gamma}^{n^*}$$

with  $n^*$  the flow behaviour index and  $m$  the flow consistency index. In case of shear thinning fluids,  $n^* < 1$  and the smaller the value of  $n^*$ , the more shear thinning is the material.

Yield stress or yield point ( $\tau_0$ ) is defined as the minimal force that must be exerted on a material to make it start flowing. Yield stress can be determined by different extrapolation and curve-fitting methods based on  $\tau$  and  $\dot{\gamma}$  [75], but the outcomes can strongly depend on the sensitivity of the measuring device, as well as give values for materials that in reality do not have a yield stress (i.e. materials that flow even when shear stress approaches zero). In this study, following the example of other bioprinting studies [27, 73], yield stress was defined as the crossover point of the storage modulus ( $G'$ ) and loss ( $G''$ ) modulus, which are measures of elastic and plastic

deformation, respectively. An oscillatory shear stress sweep was applied from 0.1 to 1000 Pa ( $\varnothing$  25 mm parallel plates, 1 Hz, 0.8 mm gap) and if present, the crossover point of  $G'$  and  $G''$  was determined using linear interpolation.

A variant of a so-called three interval thixotropy test (3ITT) was performed in PP configuration to investigate viscosity recovery from high shear. First, a constant shear of 1/s was applied for 200 seconds, since previous measurements had shown that at this shear rate the viscosity did not change over the course of ten minutes (for 5% Dex/HA 0.0030). Next, a high shear of 100/s was applied for ten seconds, followed by another 200 seconds at 1/s. Viscosity recovery was expressed as the percentage of initial viscosity, where the initial viscosity was determined by averaging over the ten seconds before high shear and the recovered viscosity by averaging over ten seconds starting 30 seconds after returning back to low shear.

Dex/HA formulations were compared to Cellink Start (Cellink), a commercial polypropylene oxide bioink.

## 2.3 Bioprinting

### *Materials*

At the Sahlgrenska Academy, bioprinting was performed using a BIO X bioprinter (Cellink) with a printhead for pneumatic extrusion printing with conical 25G polypropylene nozzle. Bioprinting at the University of Twente was performed on a INKREDIBLE+ (Cellink) pneumatic extrusion bioprinter with dual printheads. In each of the printheads, one 3 mL cartridge can be attached. Polypropylene nozzles (Cellink) were available, as well as stainless steel coaxial nozzles (Raméhart instrument co.) with 28G/22G and 26G/20G inner/outer nozzle size respectively.

### *Software*

CAD print designs were prepared in AutoCAD and Repetier-Host and sliced using Slic3r software. Manual adaptations were made to the resulting g-code, e.g. to include different printing speeds in a single print.

### *Printability assessment*

To assess the printability of pre-crosslinked Dex/HA with different degrees of crosslinking, extrusion at 10, 50, 75, 150 and 300 kPa was tested with the INKREDIBLE+ printer using a conical 22G nozzle. For each potential bioink, the three best performing pressures were selected for further printability assessment, which consisted of printing filaments of 10 mm in length at three different printing speeds: 2.5, 10 and 25 mm/s (**Figure 2a**). For each combination of extrusion pressure and printing speed (nine combinations per ink), three filaments were printed in a polystyrene petri dish. The g-code is available in the supplements (Appendix 2).

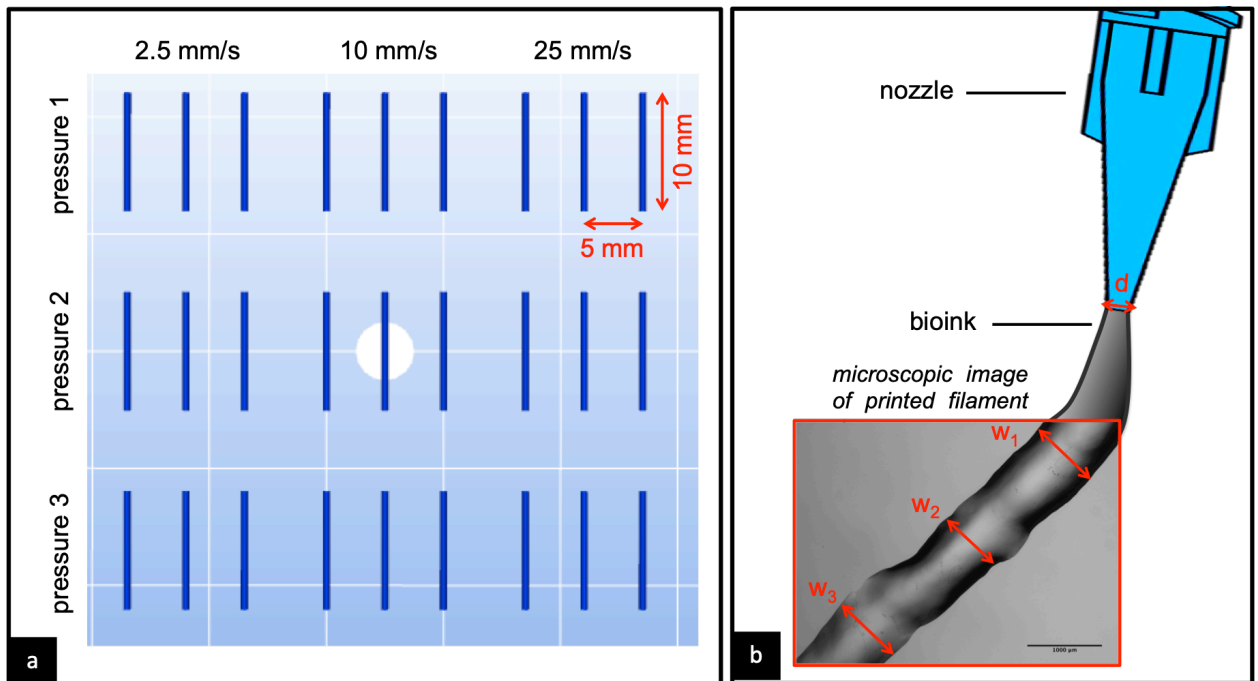


**Figure 2:** Printability assessment. **a)** Repetier Host representation of CAD file, used for printing filaments at different combinations of printing speed and extrusion pressure. **b)** The nozzle diameter ( $d$ ) and actual filament width measurements ( $w$ ) are used to calculate printing parameters: filament spread and diameter variation. The filament width is measured at three positions from microscopic images (top view).

Printability was assessed by measuring the filament width from microscopic images (Nikon TE300, 2X objective) using ImageJ software at three different positions per filament (**Figure 2b**). To determine the filament spread, the mean of these three measurements was divided by the nozzle diameter:

$$\text{spread} = \frac{(w_1 + w_2 + w_3)/3}{d}$$

As a second printability parameter, variation within a filament was defined as the standard deviation (SD) between the three width measurements as a percentage of the mean width:

$$\text{diameter variation} = \frac{SD(w_1 + w_2 + w_3)}{(w_1 + w_2 + w_3)/3} * 100\%$$

Ideally, the spread is close to 1 and the diameter variation close to zero. Criteria for 'good printability' were set at <2 for filament spread and <10% diameter variation, for 'moderate printability' at <3 for filament spread. In case of larger filament spread (overextrusion), no or

interrupted extrusion (underextrusion), the material was considered as not printable for this set of parameters. Again, Cellink Start was used as a reference material.

## **2.4 Cell culture, encapsulation and chondrogenesis**

### *iPSC culture*

Two different iPSC cell lines were cultured: the A2B line, reprogrammed from ACI-donor chondrocytes as described by Boreström et al. [59]; and the same line but genetically modified by insertion of green fluorescence protein (GFP) as a reporter gene under control of the promoter for aggrecan (ACAN). This modified cell line is referred to as 'H8' and allows detection of ACAN expression by fluorescent imaging. Both iPSC lines were cultured using Cellartis® DEF-CS™ 500 Culture System (TaKaRa Bio, Sweden). DEF-CS basal medium was supplemented with 3 µL/mL GF-1, 1 µL/mL GF-2 and 1 µL/mL GF-3. iPSCs were seeded at a density of 30.000-50.000 cells/cm<sup>2</sup>. Medium was refreshed every day and cells were passaged every 3 days using TrypLE Select or TrypLE Express (Gibco™).

### *Cell encapsulation*

The desired number of iPSCs was centrifuged, resuspended in a small volume and mixed with a high-concentration gel precursor and additional volume, to ensure that the final polymer concentration was unaltered despite the volume of the cell suspension. Subsequently, hydrogel was prepared as described earlier. For (non-bioprinted) 3D hydrogel cultures, gel precursor including iPSCs was divided into smaller volumes which were cross-linked one by one. This way, enough time was provided to transfer three individual gels into a multi-well plate by pipetting.

### *Chondrogenesis of iPSCs*

Directed chondrogenesis of H8 iPSCs was induced by chondrogenic medium consisting of high-glucose DMEM (PAA Laboratories, Cat No. E15-843), 1% penicillin/streptomycin (100X, PAA Laboratories), 1% Insulin-Transferrin-Selenium (100X, Life technologies), 100 nM dexamethasone (Sigma-Aldrich), 80 µM L-ascorbic acid (Sigma), 1 mg/mL human serum albumin (Equitech-Bio, TX, USA), 5 µg/L linoleic acid (Sigma-Aldrich), 10 ng/mL TGF-β1 (R&D Systems) and 10 ng/mL TGF-β3 (R&D Systems). The medium was refreshed every 2-3 days.

Chondrogenesis was induced for five weeks in two different types of 3D culture: (non-printed) hydrogel and pellets. iPSC pellets were obtained by centrifugation for 5 min at 700 rcf. The H8 cell line was chosen so that ACAN expression could be monitored using fluorescence imaging. To this end, hydrogels and pellets were cultured in a black 96-well plate with round clear bottom.

## 2.5 Evaluation of cellular activity and chondrogenesis

### *ACAN gene expression*

To analyse ACAN expression, fluorescence microscopy images were obtained every week using an IN Cell Analyzer 6000 (GE Healthcare) with FITC filter. A z-stack of scans was made and the resulting maximal intensity projection was saved, with contrast setting such that minimum and maximum pixel value in the image correlated to 0 and 2000 arbitrary intensity units, respectively.

### *PrestoBlue assay*

PrestoBlue™ (Invitrogen™) assay was performed every week as an alternative to direct viability assessment. This metabolic assay is based on the reduction of blue, non-fluorescent resazurin to pink, high fluorescent resorufin by metabolically active cells. The assay was performed following the manufacturer's instructions, after which absorbance was measured at 560 nm and 590 nm and normalized by subtracting the values at 595 nm from the values at 560. In addition, all values were corrected for background absorbance of PrestoBlue in medium alone.

### *Histology*

After five weeks in chondrogenic culture, Dex/HA gels with and without iPSCs were washed twice in PBS, fixated overnight using Histofix® (HistoLab®) and again washed twice in PBS. Excess PBS was removed and the samples were frozen and stored at -80°C until sectioning. Cryosectioning and histological staining were performed by the HistoCenter AB in Mölndal, Sweden. The samples were stained with Haematoxylin and Eosin (H&E) and Safranin O staining.

## 2.6 Compatibility of pre-crosslinked Dex/HA and iPSCs for bioprinting

Gravitational sedimentation of iPSCs in pre-crosslinked Dex/HA was assessed by imaging the bottom of wells containing Dex/HA in a multi-well plate. iPSCs in monolayer were incubated with Methylene Blue (1:1 diluted in DPBS) for five minutes and washed with PBS three times before trypsinization.  $10^6$  cells/mL were encapsulated in Dex/HA with 0.0025%, 0.0035% and 0.03%  $H_2O_2$ . For each condition, 3 x 350  $\mu$ L was pipetted into a 48-well plate and microscopic images were taken at the bottom of each well approximately every five minutes using a Nikon TE300 with 10X objective.

To investigate the effect of including iPSCs on the viscosity of pre-crosslinked Dex/HA,  $10^7$  cells/mL were encapsulated and subsequent viscosity measurements were performed as described before.

## 3 RESULTS

### 3.1 Creation of a viscous bioinks by enzymatic pre-crosslinking of Dex/HA

First of all, it had to be demonstrated whether it is possible to create viscous solutions by pre-crosslinking Dex/HA with a small amount of  $H_2O_2$ . Therefore, 10% Dex/HA (Dex-TA: DS15) was combined with 3.5 U/mL HRP and different  $H_2O_2$ /TA molar ratios, ranging from the optimum established for the injectable hydrogel (0.18  $H_2O_2$ /TA), down to  $1/16^{\text{th}}$  of this concentration (0.011  $H_2O_2$ /TA). In **Figure 3**, it is shown that the gelation time decreased exponentially with decreasing  $H_2O_2$ /TA ratio. It was found that for 10% Dex/HA, the addition of between  $\sim 0.018$  and  $\sim 0.030$   $H_2O_2$ /TA, which is six- to ten-fold lower than the initial ratio for injectable hydrogels, yielded viscous polymer solutions.

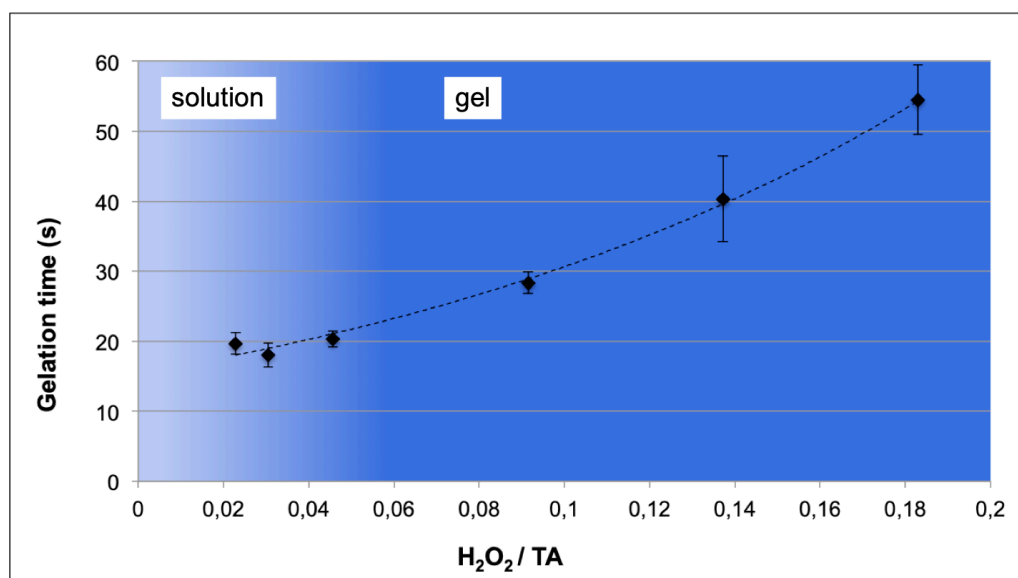


**Figure 3:** The effect of  $H_2O_2$ /TA molar ratio on gelation time and physical appearance of 10% Dex/HA with Dex-TA of DS15 and HRP concentration of 3.5 U/mL. Light blue: (viscous) solution, dark blue: gel. The dashed line presents an exponential curve fitted to the data, illustrating an exponential, positive correlation of gelation time with  $H_2O_2$ /TA ratio.  $n=3$  for each condition.

Next, the viscosity of Dex/HA pre-crosslinked within this  $H_2O_2$ /TA range was characterized. 10% Dex/HA samples were prepared from six different Dex-TA batches since, in contrast to the HA-TA batches, Dex-TA presented variability in degree of tyramine substitution (DS). The same  $H_2O_2$  concentration was used for all batches, resulting in  $H_2O_2$ /TA ratios between 0.022 for Dex-TA with DS11 to 0.028 for Dex-TA with DS16. In addition, Dex-TA batches had been synthesized

using two different methods, labelled old (O) and new (N), which was taken into consideration as well. Most Dex-TA batches resulted in a material with strong shear thinning behaviour ( $n^*$  between 0.14 and 0.25) and viscosity comparable to that of Cellink Start, a commercial bioink with optimized printability ( $n^* = 0.25$ ) (**Figure 4**). No correlation with degree of substitution was found and the synthesis procedure had no significant effect. Only one batch, synthesized according to the new method and having a DS of 13 (N/DS13), resulted in a Dex/HA solution presenting drastically lower viscosity, with a difference of up to 3 orders of magnitude at low shear rate. In addition, the solution was barely shear thinning ( $n^* = 0.96$ ).

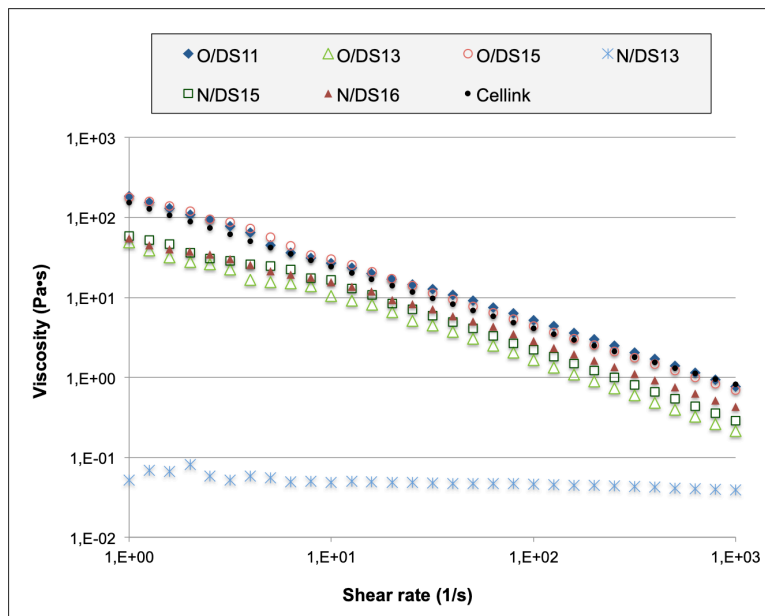


**Figure 4:** Shear viscosity of 10% Dex/HA based on different Dex-TA batches, using 3 U/mL HRP and 0.0041%  $H_2O_2$  (0.022 – 0.028  $H_2O_2/TA$ ). O: old synthesis method; N: new synthesis method; DS: degree of substitution. Cellink: Cellink Start bioink. All Dex/HA solutions present viscosity and shear thinning comparable to Cellink Start, except for the solution based on batch N/DS13. This solution is significantly less viscous and barely shear thinning.

The deviating batch was further investigated, which led to the finding that an increase in  $H_2O_2/TA$  ratio from 0.025 to 0.033 resulted in a viscosity profile and shear thinning behaviour ( $n^* = 0.24$ ) similar to that of the commercial bioink Cellink Start (**Figure 5a**). Next, it was shown that Dex/HA from this same Dex-TA batch, but using half the polymer content (5%), could be pre-crosslinked into a solution with similar viscosity profile (**Figure 5b**). This solution was even more shear thinning ( $n^* = 0.17$ ). The required  $H_2O_2/TA$  ratio to obtain viscosity like that of Cellink Start, was higher for 5% than for 10% Dex/HA:  $\sim 0.042$  compared to  $\sim 0.033$ .

To summarize, it was shown that most Dex-TA batches responded similarly to a fixed low concentration of  $H_2O_2$ . This suggests that at low  $H_2O_2/TA$  ratio, crosslinking is to a greater extent dependent on concentration  $H_2O_2$  than on  $H_2O_2/TA$  ratio. However, one batch (N/DS13) required a higher  $H_2O_2/TA$  ratio to obtain a viscous and shear thinning material. Degree of substitution and synthesis method were excluded as potential causes. Unbound tyramine groups could scavenge  $H_2O_2$ , but the NMR spectrum showed that the batch is free of such impurities. Therefore, it was assumed that the configuration and/or distribution of tyramine groups is

different from other batches. It should therefore be considered that results found using this batch do not always need to be true for other batches. For all investigated Dex-TA batches, as well as for both 5% and 10% polymer concentration, shear thinning viscosity profiles were demonstrated comparable to that of a commercial bioink, presenting a good starting point for pre-crosslinked Dex/HA as a potential bioink.

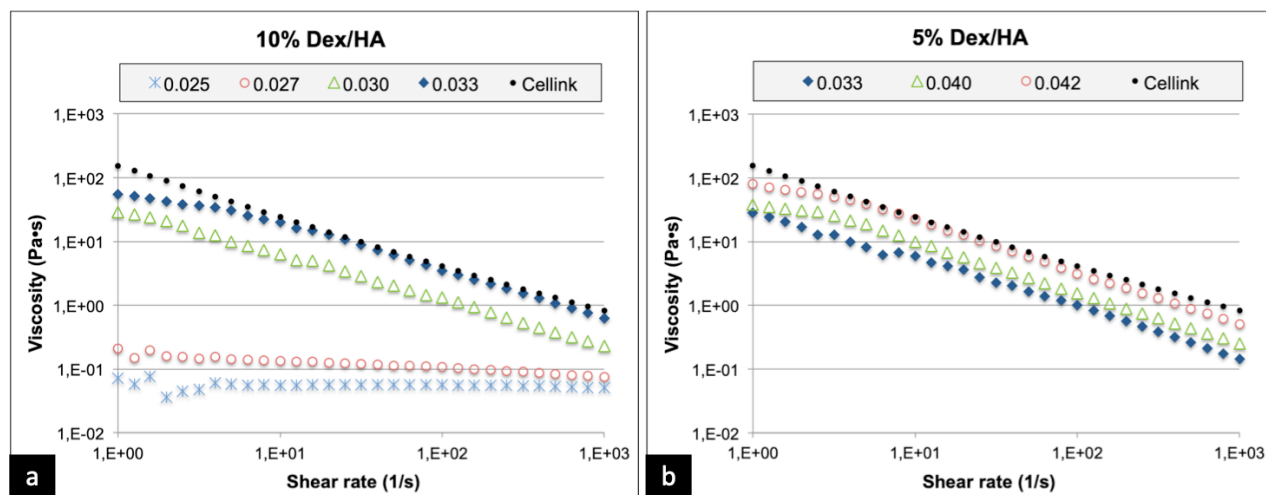


**Figure 5:** Shear viscosity of **a:** 10% Dex/HA and **b:** 5% Dex/HA based on Dex-TA N/DS13 with 3 U/mL HRP and different H<sub>2</sub>O<sub>2</sub>/TA ratios. Both graphs show that increased H<sub>2</sub>O<sub>2</sub>/TA leads to increased viscosity and that it is possible to obtain a viscosity curve similar to that of Cellink Start (black dots). Numbers in the legend indicate H<sub>2</sub>O<sub>2</sub>/TA molar ratio.

Unless indicated otherwise, all further experiments were executed using Dex/HA based on batch N/DS13, 5% polymer concentration and 1 U/mL HRP; therefore these features will be omitted in Dex/HA notations. The N/DS13 batch was selected because of its large availability, despite its deviating behaviour. The rationale behind using 5% polymer concentration was to promote cell migration and reduce material consumption. Based on the experience within the research group, it was assumed that reducing HRP concentration from 4 to 1 U/mL would not have any significant effect on the crosslinking end result, while it poses the advantage of a longer handling time, e.g. for mixing in cells or filling a cartridge. It was also investigated whether PBS could be replaced by the DMEM forming the base of the chondrogenic differentiation medium, but this appeared to delay the crosslinking process and require higher H<sub>2</sub>O<sub>2</sub>/TA ratios (supplementary data, **Table S2**). Considering these significant effects, which were attributed to the presence of H<sub>2</sub>O<sub>2</sub>-scavenging medium components, only PBS was used in further experiments.

### 3.2 Rheological properties of pre-crosslinked Dex/HA

The relationship between the amount of H<sub>2</sub>O<sub>2</sub> and the shear viscosity was characterized using viscosity measurements in double gap configuration (**Figure 6**). In general, it can be observed

that increasing the H<sub>2</sub>O<sub>2</sub> level leads to an increase in viscosity, although this is not evident for higher H<sub>2</sub>O<sub>2</sub> levels (0.040 – 0.047 H<sub>2</sub>O<sub>2</sub>/TA) at low shear rate (up to ~10/s). A comparison of the viscosity of Dex/HA with 0.040 H<sub>2</sub>O<sub>2</sub>/TA, prepared and measured at different dates, points out a lack of reproducibility (**Figure 7**). Disregarding viscosity at low shear, the viscosities differ up to one order of magnitude (22-mrt compared to 23-apr). Two out of five Dex/HA solutions (10-jul and 12-jul) appear to have an infinite viscosity when approaching zero shear rate and remarkably, display a region with viscosity increase at high shear. The other three exhibit a viscosity plateau at low shear.

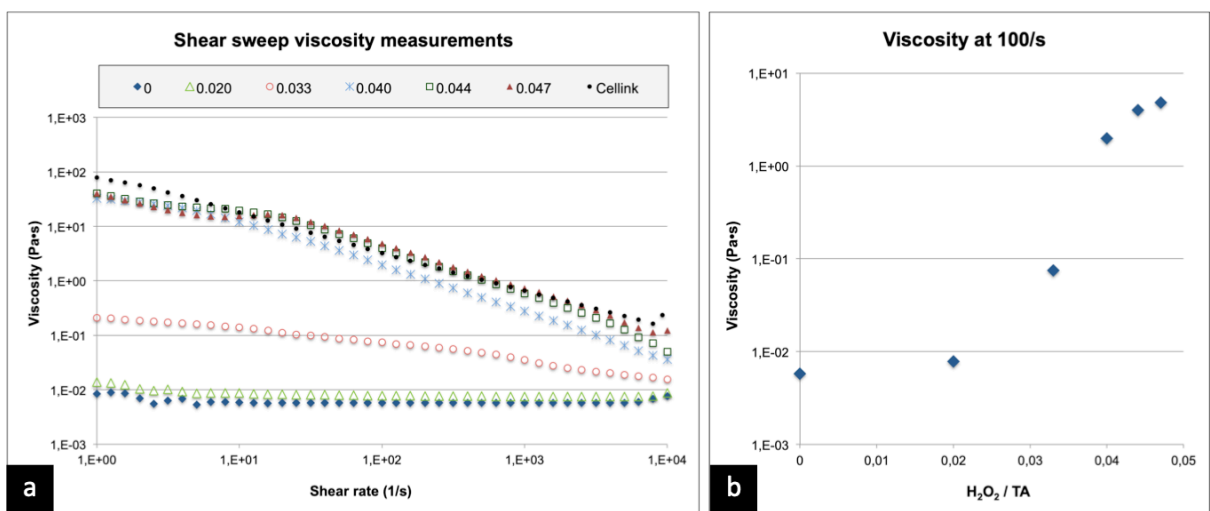


**Figure 6:** Relationship between H<sub>2</sub>O<sub>2</sub>/TA ratio and the shear viscosity of 5% Dex/HA (Dex-TA: N/DS13) with 1 U/mL HRP. **a:** Apparent viscosity during a shear rate sweep from 1/s to 10,000/s for different H<sub>2</sub>O<sub>2</sub>/TA ratios, indicated by the numbers in the legend. **b:** Shear viscosity during shear sweep at 100/s as a function of H<sub>2</sub>O<sub>2</sub>/TA ratio. Viscosity is positively correlated with H<sub>2</sub>O<sub>2</sub>/TA ratio and above 0.02 H<sub>2</sub>O<sub>2</sub>/TA, shear thinning occurs. At higher H<sub>2</sub>O<sub>2</sub>/TA ratios of >0.04, the viscosity increase seems to reach a plateau.

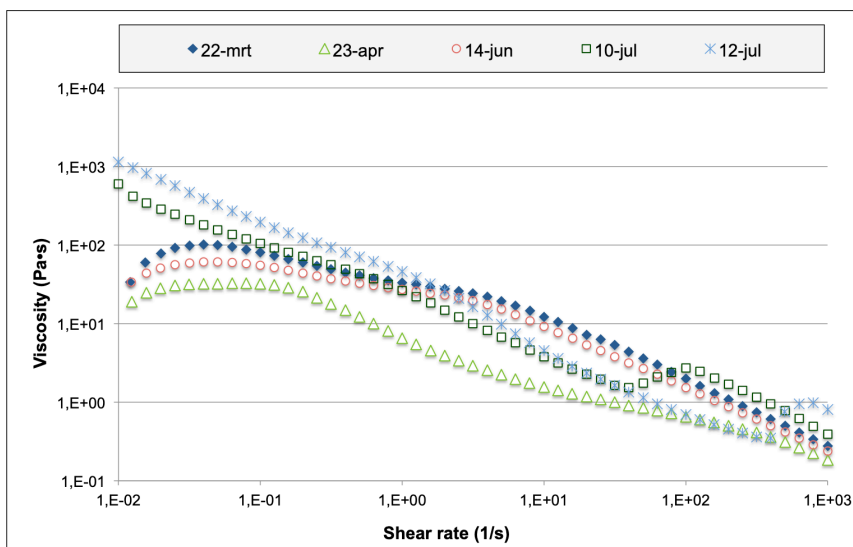


**Figure 7:** Shear viscosity of Dex/HA 0.040 prepared and measured at individual dates (as indicated in the legend). Differences between the samples can be observed regarding overall viscosity, behaviour at low shear and behaviour at high shear.

When a series of shear sweep measurements was performed, it was observed that during the first measurement the viscosity was much higher than during subsequent measurements, while temperature had only a minor effect (**Figure 8a**). This viscosity drop after the first shear sweep was also present when there was a zero shear period of up to ~7 minutes in between the measurements (required for reaching thermal equilibrium when the temperature was adjusted). The phenomenon was only observed for crosslinked Dex/HA, but appears not to be proportional to the degree of crosslinking, since the reduction in viscosity was most pronounced at H<sub>2</sub>O<sub>2</sub>/TA ratios of 0.040 and 0.044 (**Figure 8b**).

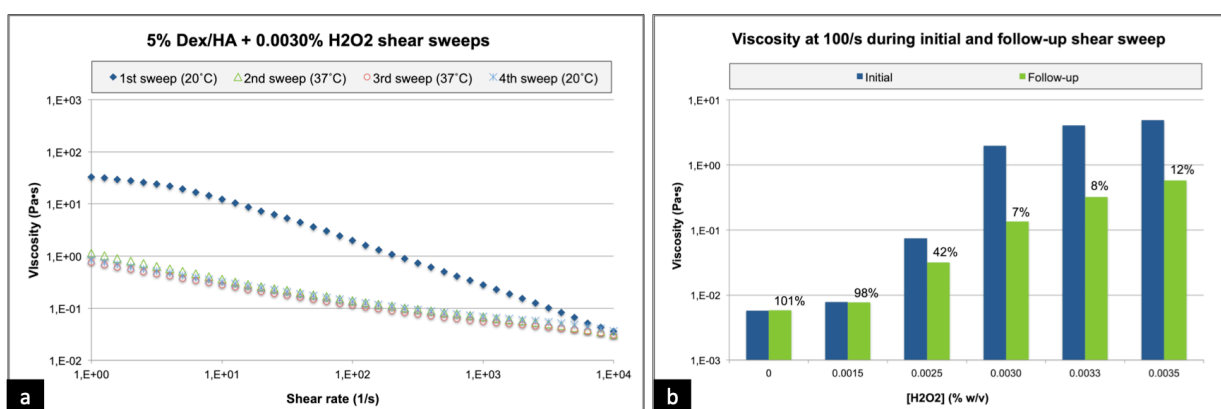


**Figure 8:** Viscosity measurements showing the effect of shear history on viscosity of pre-crosslinked Dex/HA. **a:** Subsequent shear sweep measurements on 20°C and 37°C show a major viscosity drop between the first and second measurement. Between the second and third shear sweep, here both at 37°C, only a minor decrease is observed. The fourth shear sweep at 20°C shows a minor increase compared to the third. **b:** Viscosity at 100/s shear rate during initial and follow-up shear sweep measurements, both at 20°C. Follow-up was the fourth shear sweep for Dex/HA with 0.040 H<sub>2</sub>O<sub>2</sub>/TA, third shear sweep for all other conditions. In the graph, follow-up viscosity at 100/s is expressed as a percentage of the initial viscosity.

To further investigate this shear history-dependent behaviour, 3ITT was performed for Dex/HA 0.040, 0.044 and 0.047. As expected from the shear thinning behaviour previously demonstrated, viscosity drops for all conditions when the shear rate is increased from 1/s to 100/s (**Figure 9**). In addition, for Dex/HA 0.044 and 0.047, the viscosity keeps decreasing throughout the period of high shear. Upon returning to low shear, viscosity initially rises – for 0.040 even above the initial value – followed by a decrease within seconds. In case of the two highest H<sub>2</sub>O<sub>2</sub> concentrations, a slight increase is observed afterwards. All Dex/HA viscosities seem to stabilize more or less within 30 seconds at a level significantly lower than the initial viscosity. The percentage of recovery decreases with increased degree of crosslinking. In contrast to Dex/HA, the viscosity of Cellink Start is recovered almost completely (99%) within ten seconds after returning to low shear.

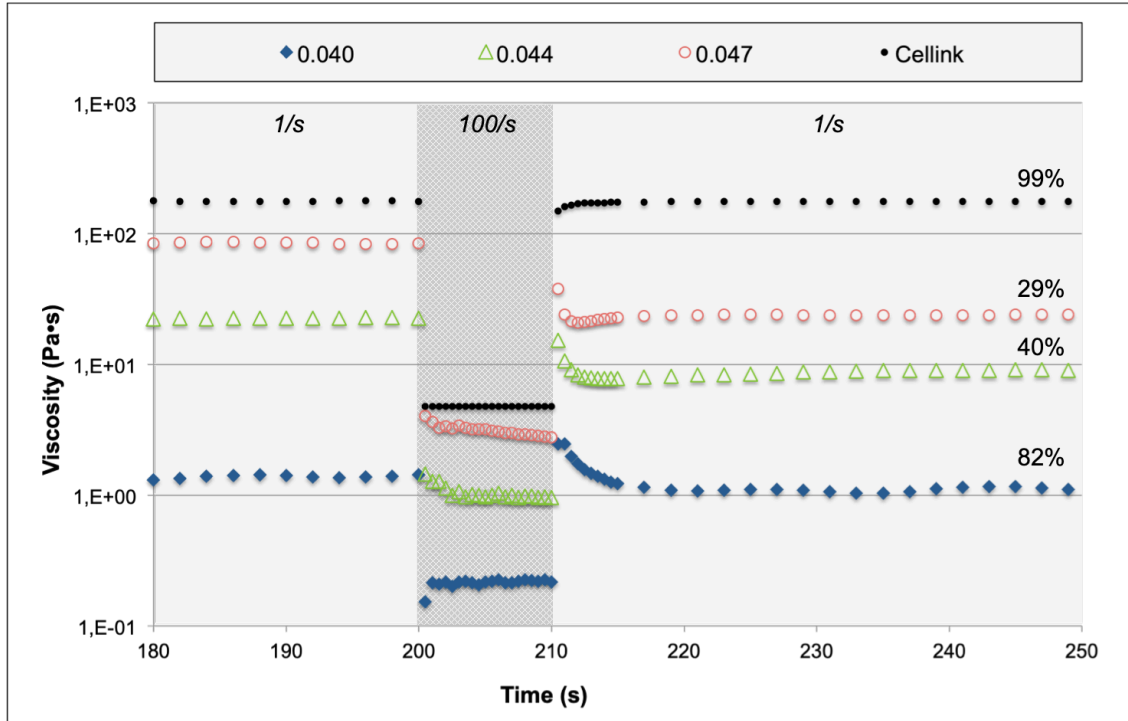


**Figure 9:** Three interval thixotropy test showing the response of pre-crosslinked Dex/HA to high shear. First, a period of low shear (1/s) is applied during which viscosity is more or less constant for all conditions. Next, high shear of 100/s is applied for ten seconds (dark grey), leading to an immediate viscosity drop. After returning to 1/s, viscosities increase but not to the same level as initially before high shear. The recovery after 30s expressed as percentage of initial viscosity at 1/s, is displayed.

### 3.4 Printability of pre-crosslinked Dex/HA

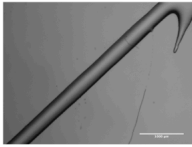
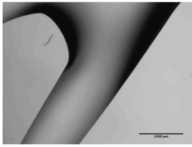
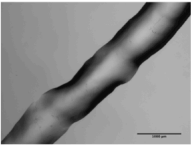
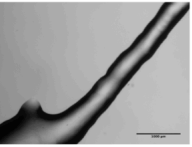
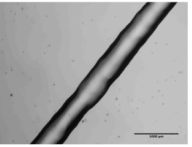
Based on the rheological characterization, Dex/HA 0.033, 0.040, 0.044 and 0.047 were selected for printability assessment, of which the results are presented in **Figure 10**. As was expected from its low viscosity and shear thinning ability, Dex/HA 0.033 was not printable, since it could not provide shape fidelity. For the other Dex/HA formulations, good or reasonable printability was achieved for at least one extrusion pressure. However, compared to Cellink Start the required pressure was higher and the pressure range for printability was smaller. It is also notable that Dex/HA 0.044 could not be extruded at 75 kPa, while Dex/HA 0.040 and 0.047 could. This was considered to be an outlier,

The results of the printability assessment are summarized in **Table 1**. The printing parameters that yielded optimal printability are presented, as well as a microscopic image of the best result for each bioink. From these images it becomes clear that Cellink Start not only yields high resolution, but also a constant filament width and smooth filament edges. Reasonable accuracy can be achieved with Dex/HA formulations, but the extrusion is less constant, resulting in less smooth filaments. Note that viscosity and flow behaviour index are measured on the exact same material that was printed, but not the yield stress and recovery from shear

	10 kPa	50 kPa	75 kPa	150 kPa	300 kPa
Cellink Start	Printable with filament spread <200% and diameter variation <10%	Printable with filament spread <200% and diameter variation <10%	Printable with filament spread <200% and diameter variation <10%	Printable with filament spread of 200-300% and/or diameter variation >10%	Overextrusion (filament spread >300%)
Dex/HA 0.033	Underextrusion (no or interrupted extrusion)	Underextrusion (no or interrupted extrusion)			
Dex/HA 0.040	Underextrusion (no or interrupted extrusion)	Underextrusion (no or interrupted extrusion)	Printable with filament spread <200% and diameter variation <10%	Printable with filament spread of 200-300% and/or diameter variation >10%	Underextrusion (no or interrupted extrusion)
Dex/HA 0.044	Underextrusion (no or interrupted extrusion)	Underextrusion (no or interrupted extrusion)	Underextrusion (no or interrupted extrusion)	Printable with filament spread of 200-300% and/or diameter variation >10%	Underextrusion (no or interrupted extrusion)
Dex/HA 0.047	Underextrusion (no or interrupted extrusion)	Underextrusion (no or interrupted extrusion)	Printable with filament spread <200% and diameter variation <10%	Printable with filament spread of 200-300% and/or diameter variation >10%	Underextrusion (no or interrupted extrusion)

**Figure 10:** Printability assessment of Dex/HA bioinks at different extrusion pressures. The results are rated with good (green), moderate (yellow) or no (red) printability, based on the criteria as described in the legend.

**Table 1:** Optimal parameters and results of printability assessment and rheological bioink properties. The microscopic images (2X objective) show the best print result for each tested bioink; corresponding printing parameters and filament spread ( $\pm$  standard deviation) are stated in the upper three rows. A summary of rheological properties is listed in the lower four rows. N.a. = data not available. Scale bars: 1000  $\mu$ m.

	CELLINK Start	Dex/HA 0.033	Dex/HA 0.040	Dex/HA 0.044	Dex/HA 0.047
<b>Pressure (kPa)</b>	75 kPa	10 kPa	75 kPa	150 kPa	75 kPa
<b>Print speed (mm/s)</b>	25 mm/s	25 mm/s	10 mm/s	25 mm/s	10 mm/s
<b>Filament spread</b>	0.93 $\pm$ 0.04	3.24 $\pm$ 0.49	1.96 $\pm$ 0.26	1.55 $\pm$ 0.49	1.23 $\pm$ 0.23
<b>Microscopic image</b>					
<b>Viscosity at 10/s (Pa*s)</b>	2.51	0.075	1.89	4.02	4.84
<b>Flow behaviour index</b>	0.25	0.74	0.14	0.16	0.19
<b>Viscosity recovery from shear (%)</b>	99	n.a.	82	40	29
<b>Yield stress (Pa)</b>	233	n.a.	110	83	352

To assess the effect of poor pre-crosslinking reproducibility as demonstrated in **Figure 7**, the viscosity of three Dex/HA 0.040 solutions prepared at three different dates was compared to the minimal required extrusion pressure through the inner (26G) nozzle of a 26G/20G coaxial nozzle. Note that 25G and 26G have the same inner diameter, but the geometry and material of this nozzle is different from the 25G polypropylene nozzle used for **Figure 10/Table 1**. Because of the major permanent viscosity loss observed in pre-crosslinked Dex/HA, viscosity during the final shear sweep measurement for each sample was considered to be the most representative for the printed material. The full shear sweeps are included in the supplementary data (**Figure S1**) and the viscosity at 100/s is stated in **Table 2**. Minimal extrusion pressure was positively correlated to viscosity. The most viscous Dex/HA solution (12-07) was not extrudable even at the upper pressure limit of the INKREDIBLE+ bioprinter (300 kPa).

**Table 2:** Relating the viscosity and printability of Dex/HA 0.040 solutions prepared on different dates. Viscosity was positively correlated with required extrusion pressure (26G straight nozzle).

Crosslinking date	Viscosity at 100/s (Pa*s)	Extrusion pressure (kPa)
18-06	0.219	200
10-07	0.694	250
12-07	0.787	>300 (no extrusion)

Using one of these samples (10-07), 3D printing potential was demonstrated by the creation of a  $\varnothing$  5 mm hollow cylinder of  $\pm 15$  layers and several mm in height without wall collapse (**Figure 11**). However, extrusion was quite inconsistent, which was compensated by the use of a small layer height, enabling the layer to stay connected even when extrusion is briefly interrupted.

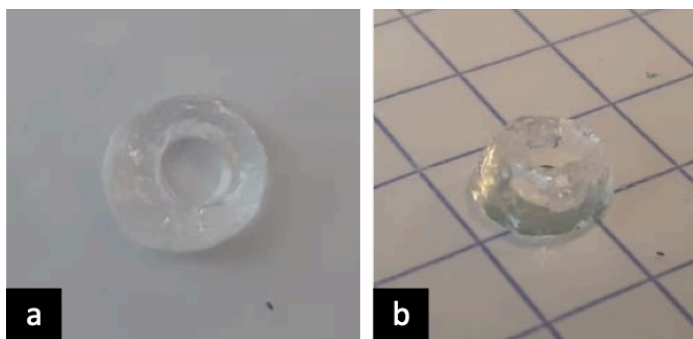


**Figure 11:** Top view (a) and side view (b) of 3D-printed hollow cylinder using Dex/HA 0.040. The grid placed underneath the construct in b consists of 5x5 mm squares.

To obtain a stable construct that maintains its shape and provides mechanical cues to residing cells, post-crosslinking after printing was desired. This was demonstrated for 10% Dex/HA based on Dex-TA batch O/DS15, pre-crosslinked with 0.023 H<sub>2</sub>O<sub>2</sub>/TA. One-layer structures printed

using the BIOX printer were immersed in 0.03%  $H_2O_2$  for 15 minutes, which demonstrated enhanced gel density and shape preservation (**Figure 12**). In contrast, immersion of printed structures in PBS without crosslinking agent, resulted in gel instability.

Considering all of these findings, it was shown that enzymatic pre-crosslinking, printing and post-crosslinking of Dex-HA is feasible, but the current procedure yielded poorly reproducible rheological properties and printing results. The viscosity and degree of shear thinning of pre-crosslinked Dex/HA seem appropriate for printing, but heterogeneous crosslinking and permanent viscosity loss presented less favourable characteristics.

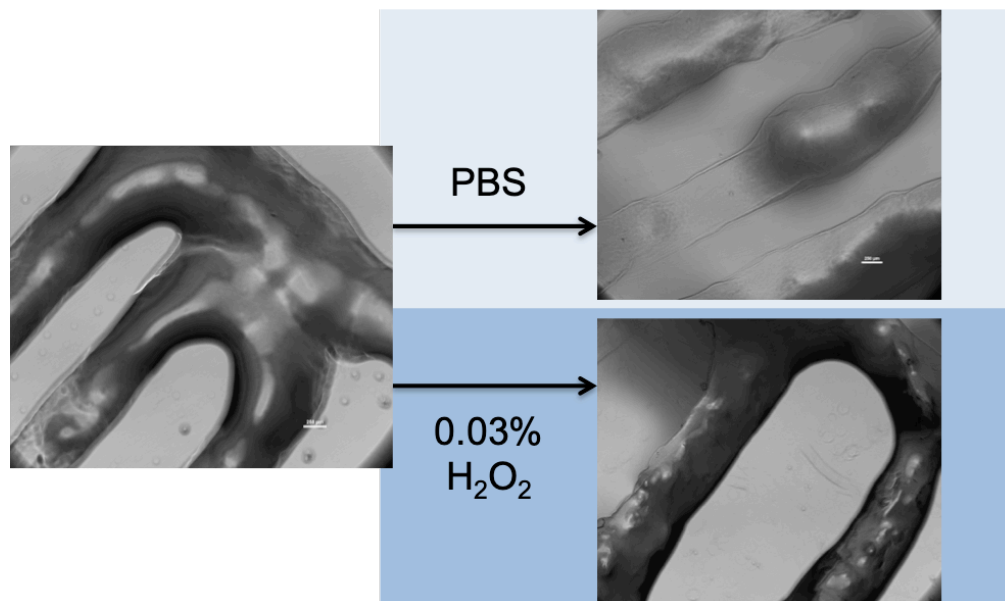


**Figure 12:** Microscopic images of 1-layer lattices printed with 10% Dex/HA 0.023 (top view). Left: directly after extrusion. Top right: after incubation with PBS. Bottom right: after post-crosslinking with 0.03%  $H_2O_2$ . It can be observed that immersion in PBS destabilizes the printed construct, while immersion in 0.03%  $H_2O_2$  leads to apparently increased gel density and better preservation of shape. Scale bars: 250  $\mu m$

### 3.4 Effect of Dex/HA gel composition on iPSC metabolism and ACAN expression

So far, focus had been on the printability of pre-crosslinked Dex/HA. However, the bioactivity of the material is equally important for achieving a successful cartilage tissue engineering strategy. To gain more insight into the effect of Dex/HA on iPSC viability and chondrogenesis, the effect of different gel compositions was investigated. It was hypothesized that lowering the polymer concentration of Dex/HA gels would enhance iPSC viability and chondrogenesis, since it is known that high polymer concentration can hamper cell viability and migration, and cell-cell communication has shown to be important for the iPSCs [33, 71]. In addition to varying the

polymer concentration, Dex/HA gels were based on different solvents. Cell culture media-based gels were expected to outperform the standard PBS gels, due to the presence of nutrients and signalling factors, while ddH<sub>2</sub>O was expected to negatively affect iPS viability.

iPSCs were encapsulated in Dex/HA gel based on PBS, DMEM, Matrigel and ddH<sub>2</sub>O while maintaining a fixed Dex/HA polymer concentration of 10%. To study the effect of polymer concentration, iPSCs were encapsulated in 2.5%, 5% and 10% Dex/HA based on PBS. As a control, Dex/HA gels without cells were included, as well iPSC pellet cultures. Additionally, iPSCs were encapsulated in alginate and NFC/alginate, but both those control conditions were lost within a few days because the calcium level was not maintained, resulting in alginate disintegration. Except for the cell-free controls each sample contained  $2 \cdot 10^5$  iPSCs, pelleted or in 25  $\mu$ L Dex/HA.

Due the fact that common viability assays are incompatible with Dex/HA, PrestoBlue assay was used as a method to estimate cell viability. However, no significant resazurin conversion by iPSCs encapsulated in Dex/HA could be detected with absorbance measurements, even when assay sensitivity was enhanced by increasing the incubation time and PrestoBlue dilution (supplementary data, **Figure S2**). In additional experiments, significant resazurin conversion was demonstrated after 24h PrestoBlue incubation of iPSCs in both pellet culture and suspension (supplementary data, **Figure S3**). The detected conversion by iPSCs in suspension was  $\sim 2.5$  as high as by iPSCs in pellet culture. Follow-up experiments showed in addition that long term presence of PrestoBlue in culture medium is detrimental to iPSC pellet cultures (supplementary data, **Figure S4**). Most importantly, the viability or metabolic activity of iPSCs in Dex/HA could not be quantified.

After one week, increased ACAN-GFP signal could be observed in all experimental conditions compared to day 1 and compared to cell-free control (**Figure 13**). GFP signal increased each week up to five weeks, when the samples were harvested for histology. No notable differences between the different conditions can be observed, except for a slightly lower expression in Dex/HA with 2.5% polymer concentration. In the pellet culture, ACAN-GFP expression was detected starting after two weeks (data not shown) and increased each week, but the signal remained weak compared to the experimental conditions with iPSCs in Dex/HA.

Histology of samples after five weeks (n=1 per condition) of chondrogenic culturing show the presence of cells with rounded morphology in all conditions (**Figure 14**). Hydrogel rupture due to the cryosectioning procedure is visible in all cases and was not improved by the presence of cells (**Figure S5**). Dex/HA with only 2.5% polymer concentration was very soft and therefore difficult to harvest for histology. Matrix staining is clearly less intense for the PBS 2.5% gel (**Figure 14a+d**)

compared to all other conditions. DMEM, Matrigel and PBS 5% seem to present poor hydrogel integrity, but histology of cell-free controls show that with these compositions proper hydrogel formation could be achieved and kept throughout five weeks (supplementary data, **Figure S5**).

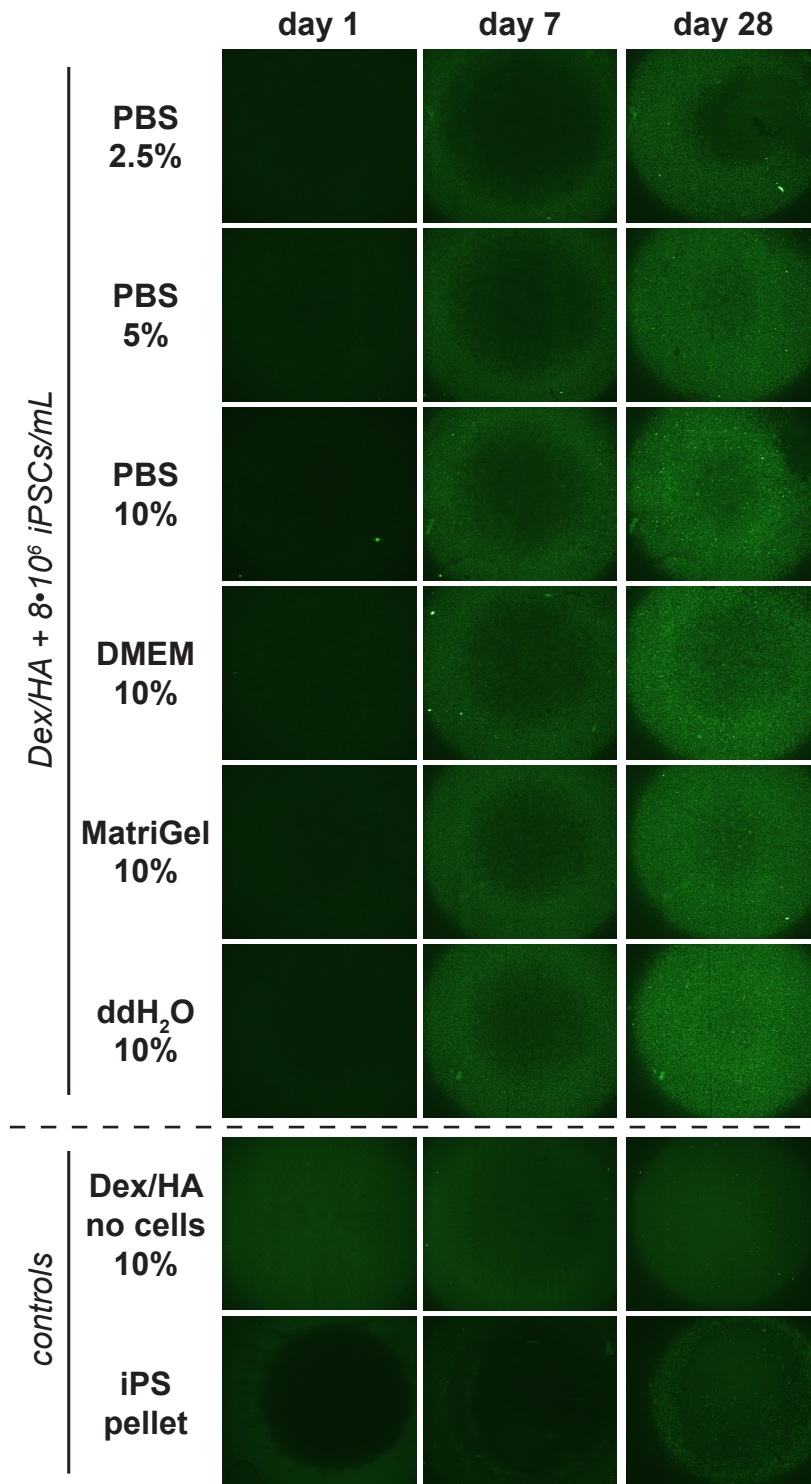


**Figure 13:** Fluorescent microscopic images of ACAN-GFP expressed by iPSCs in Dex/HA after 1, 7 and 28 days. The influence of polymer concentration (2.5, 5 or 10%) and solvent (PBS, DMEM, Matrigel or ddH<sub>2</sub>O) was investigated. Cell-free Dex/HA gels and iPSCs in pellet culture were used as negative and positive control for ACAN expression, respectively.

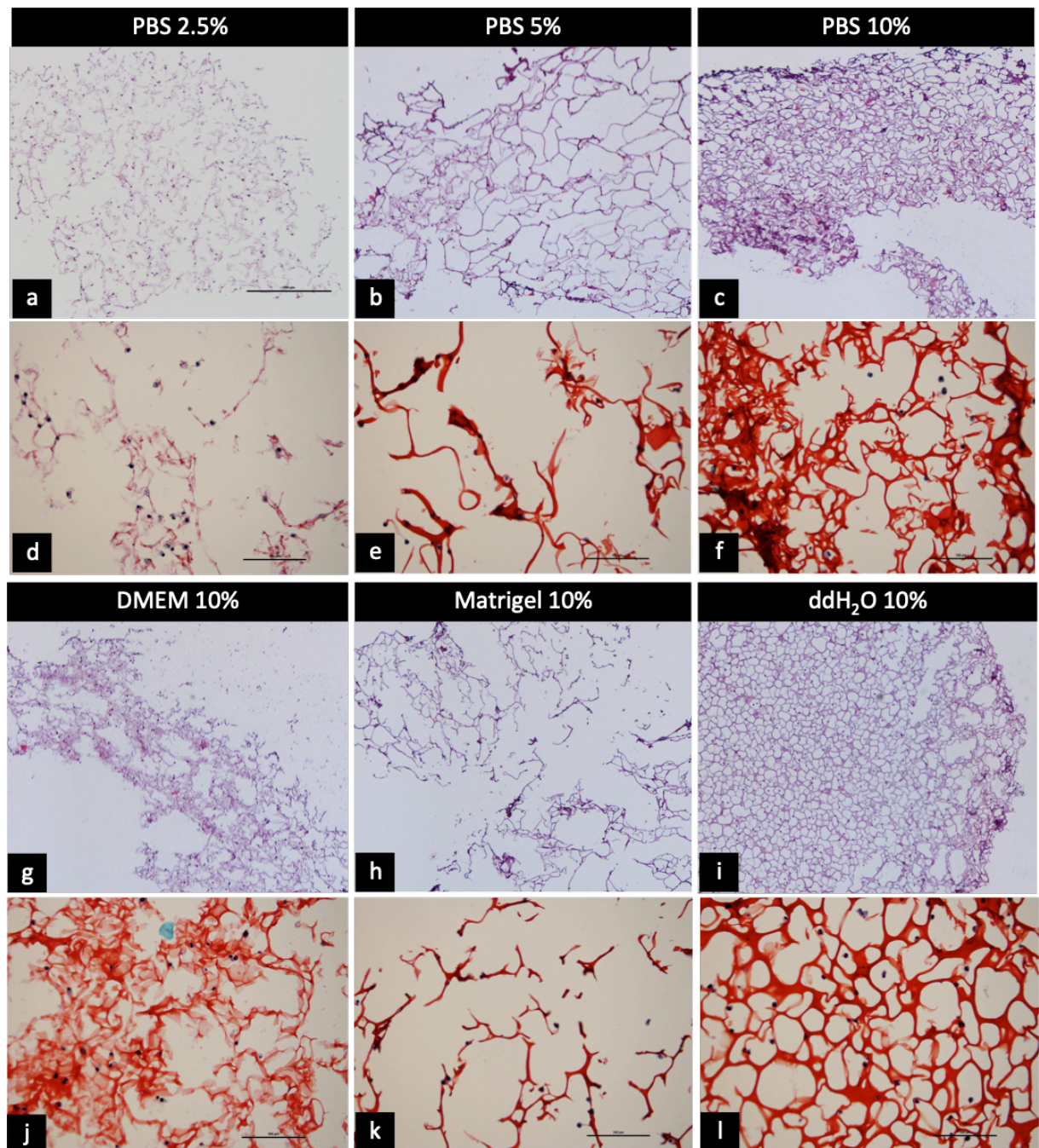


**Figure 14:** Histology of iPSCs encapsulated in Dex/HA after 35 days. Sections with H&E staining (4X objective) present an overview of the Dex/HA gel structure and distribution of iPSCs (a-c and g-i). Safranin O/fast green staining at high magnification (20X objective) shows the morphology of cells (green), nuclei (dark purple), while Dex/HA is stained in red (d-f and j-l). a-f: Gel based on PBS, a,d: 2.5% Dex/HA concentration; b,e: 5% Dex/HA concentration; c,f: 10% Dex/HA concentration. g,j: Gel based on DMEM, 10% Dex/HA concentration. h,k: Gel based on Matrigel, 10% Dex/HA concentration. i,l: Gel based on ddH<sub>2</sub>O, 10% Dex/HA concentration. Scale bar a, applicable for a-c and g-i: 500 μm. Scale bar d-f and j-l: 100 μm.

### 3.5 Combining pre-crosslinked Dex/HA bioink with iPSCs

Eventually, the aim is to print a bioink which is loaded with cells. Important properties of the bioink, as well as cell function, depend on interactions between hydrogel and cells. Among these are the total bioink viscosity, distribution of cells and shear stress experienced by cells, the latter being crucial for cell viability [24, 76].

Cell sedimentation in pre-crosslinked Dex/HA with low viscosity (0.033 H<sub>2</sub>O<sub>2</sub>/TA) and high viscosity (0.047 H<sub>2</sub>O<sub>2</sub>/TA) were compared to fully gelled Dex/HA (0.18 H<sub>2</sub>O<sub>2</sub>/TA). At t=0, approximately 1 – 2 minutes after crosslinking, a higher cell density was already visible at the bottom of Dex/HA 0.033 (**Figure 15c**) compared to the other two conditions (**Fig. 15a+b**). After ten minutes, the number of cells at the bottom of Dex/HA had increased (**Fig. 15f**), indicating cell sedimentation, while no increase was observed for the other two conditions (**Fig. 15d+e**).

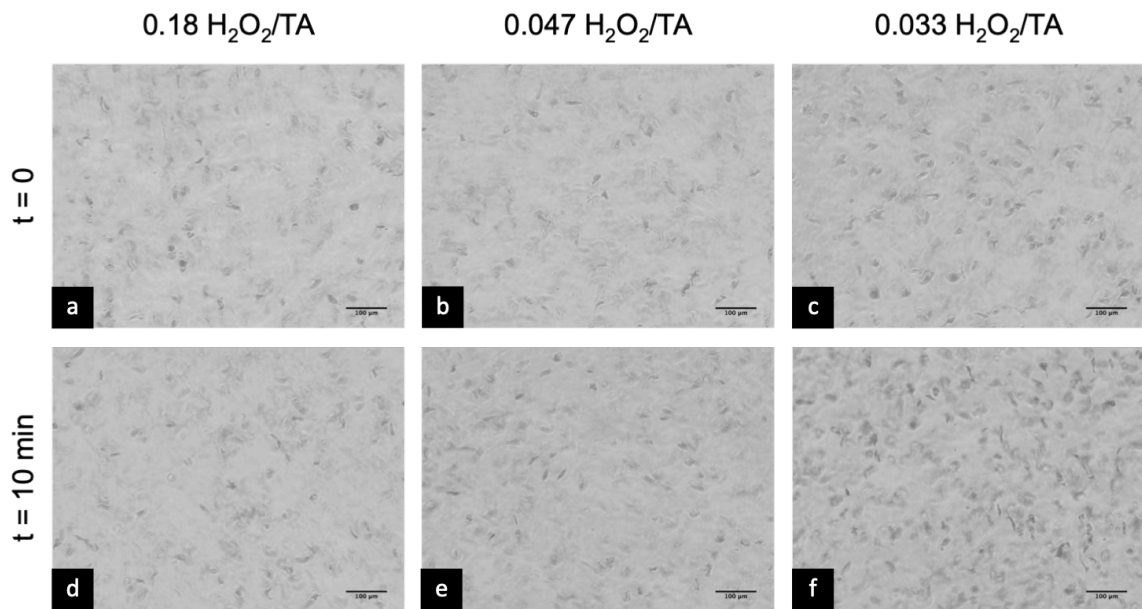


**Figure 15:** Assessment of gravitational sedimentation of iPSCs in 5% Dex/HA with different degrees of crosslinking. In solid (**a+d**: Dex/HA 0.18) and highly viscous (**b+e**; Dex/HA 0.047) gels no sedimentation is visible, while an increased cell number is observed at the bottom of Dex/HA 0.033 (**c+f**) after ten minutes. Scale bars: 100  $\mu\text{m}$

Next, the effect of encapsulating iPSCs on the viscosity of pre-crosslinked Dex/HA was investigated. When  $10^7$  iPSCs per mL were mixed with gel precursor prior to crosslinking, considered optimal for homogeneous cell mixing in the bioink, the viscosity of Dex/HA 0.040 drastically decreased compared to cell-free material and was not shear thinning (**Figure 16**). When the same concentration of iPSCs was mixed with Dex/HA 0.040 after crosslinking of the gel precursor, viscosity was more similar to and slightly higher than cell-free Dex/HA.

However, when  $10^7$  iPSCs were mixed in 10% Dex/HA, Dex-TA batch O/DS15, pre-crosslinked with 0.023  $\text{H}_2\text{O}_2$ /TA, still a viscous solution was obtained (no rheological data available). This might be attributable to the high polymer concentration. Using this cell-laden bioink, dots were printed with the INKREDIBLE+ printer (25G, 40 kPa extrusion for 2.5 seconds). The prints were post-crosslinked with 0.03%  $\text{H}_2\text{O}_2$  and kept in chondrogenic culture for nine days, after which the bioprinted samples (n=2) were harvested for histological analysis. This showed regular hydrogel structure and homogeneous distribution of iPSCs (**Figure 17**). Cell viability was not assessed since, as explained before, no suitable method had been established to do so.

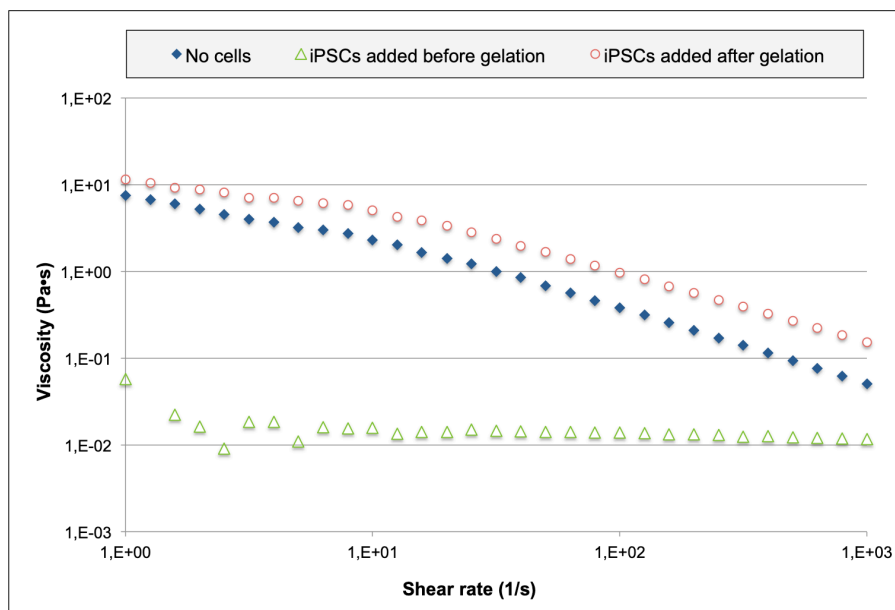


**Figure 16:** Viscosity of Dex/HA 0.040, with or without  $10^7$  iPSCs/mL mixed during or after crosslinking. When iPSCs are added before crosslinking, they have a detrimental effect on the crosslinking, resulting in a non-viscous material.

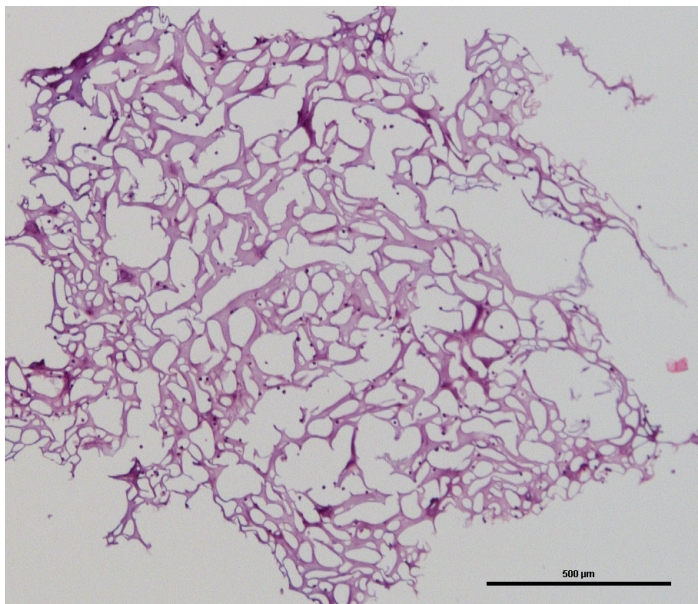


**Figure 17:** H&E staining of bioprinted Dex/HA with iPSCs ( $10^7$ /mL) presents similar structure of hydrogel (stained pink) as in non-printed hydrogels. iPSCs (purple) are homogeneously distributed throughout the gel. Scale bar: 500  $\mu\text{m}$ .

## 4 DISCUSSION

### 4.1 Enzymatic pre- and post-crosslinking of Dex/HA

It was demonstrated for the first time that enzymatic crosslinking of Dex/HA can be used to create viscous, shear thinning polymer solutions, of which the viscosity can be tuned by the concentration of the crosslinking agent,  $H_2O_2$  (**Figure 4, 5 6**). Using a decreased  $H_2O_2$  concentration for the crosslinking of Dex/HA resulted in decreased viscosity, but also in decreased gelation time (**Figure 3**). This is often explained the other way around, attributing the delay of crosslinking to HRP-inactivation by  $H_2O_2$  [77, 78]. Substrates such as tyramine are nonetheless able to compete with this inactivation, so at unsaturated  $H_2O_2/TA$  ratio levels, as used here, it was not expected to have such a large impact [79]. However, it might be related to the concentration of HRP, which was kept constant to maintain a constant HRP/TA ratio. The effect of HRP/ $H_2O_2$  ratio on gelation time at low  $H_2O_2/TA$  ratios might be worth investigating.

The rapid crosslinking at low  $H_2O_2$  levels is probably one of the factors contributing to the heterogeneous and poorly reproducible crosslinking (**Figure 7**) of viscous Dex/HA solutions. It is still not fully clear whether the lack of reproducibility is an intrinsic consequence of the hydrogel-crosslinking system or that external factors such as temperature or pipetting accuracy have an increased impact at these low levels of crosslinking, posing higher sensitivity compared to crosslinking into a solid gel. If in follow-up investigation, external factors can be identified as the major cause and a feasible way can be found to control these factors, pre-crosslinked Dex/HA still holds high potential as a stand-alone bioink. If not, Dex/HA could still be used for bioprinting, but the bioink composition and/or crosslinking modality should be altered, such that either appropriate pre-printing viscosity is achieved using a different approach, or the pre-printing viscosity of Dex/HA is no longer a crucial factor for printability. The latter can for example be achieved by instant ionic crosslinking of alginate after printing, or the use of a support material.

Interestingly, the DS of Dex-TA did seem not to have a significant effect on the viscosity (**Figure 4**). This suggests that at low  $H_2O_2/TA$  ratio, crosslinking is to a much greater extent dependent on concentration  $H_2O_2$  than on  $H_2O_2/TA$  ratio. This poses a practical advantage, because it means that there is no need for optimization of  $H_2O_2$  concentration for each individual polymer batch.

The feasibility of secondary enzymatic crosslinking of bioprinted Dex/HA was demonstrated as well (**Figure 12**). However, the mechanical and rheological properties of the resulting material were not quantified. In further research, the storage modulus and compressive modulus of

Dex/HA after enzymatic crosslinking in one step versus two steps (pre- and post-crosslinking) should be compared. This might lead to insights for optimization of the H<sub>2</sub>O<sub>2</sub> concentration of the post-crosslinking solution and the incubation time, which were now chosen more or less arbitrary.

#### 4.2 Rheological properties of pre-crosslinked Dex/HA

An ideal bioink is shear thinning, recovers rapidly after stress is released, and possesses a yield stress, although this should not be too high (i.e., crossover of G' and G'' <1000 Pa [27]). The viscosity and shear thinning of especially Dex/HA (5%; Dex-TA N/DS13) combined with 0.040 to 0.047 H<sub>2</sub>O<sub>2</sub>/TA matched very well with that of a commercial bioink (**Figure 6**). Less favourable is the thixotropic behaviour of pre-crosslinked Dex/HA including permanent viscosity loss, since this could impair post-printing shape fidelity. After two or three shear sweeps up to a shear rate of 10<sup>4</sup>/s, viscosity loss was largest (93%) for Dex/HA 0.040 (**Figure 8**), while the viscosity loss after 3ITT with short-term shear at 100/s increased with increasing H<sub>2</sub>O<sub>2</sub>/TA ratio, and thus largest loss (71%) was found for Dex/HA 0.047 (**Figure 9**). However, in all cases, the connection between H<sub>2</sub>O<sub>2</sub> increase and viscosity increase remains also after shear, which indicates that TA-TA crosslinks remain intact.

Several processes are likely to contribute to the rheological behaviour of pre-crosslinked Dex/HA. The presence of pure, time-independent shear thinning can be concluded from the fact that there is an immediate viscosity drop when shear rate rises from 1/s to 100/s and an immediate rise when the shear rate returns to 1/s (**Figure 9**). Shear-thinning is a result of reversible polymer disentanglement and alignment in the direction of shear flow. Because of the expected high level of interaction inside Dex/HA, new interactions and entanglements can be formed during the aligned state under shear, of which some are stable enough not to be reversed when stress is released, leading to a higher state of alignment and therefore lower intrinsic viscosity. The higher the crosslinking density of a polymer network, the less is the freedom of motion. Therefore, the ability of Dex/HA to align and disentangle presumably decreases with increasing H<sub>2</sub>O<sub>2</sub> concentration. By connecting different polymer chains, crosslinks effectively increase the molecular weight, which increases the risk of polymer rupture [80]. This can explain why higher H<sub>2</sub>O<sub>2</sub> concentration leads to higher permanent viscosity loss in the 3ITT. At very high shear, however, it is hypothesized that full alignment and disentanglement are achieved, after which polymer rupture occurs in all Dex/HA conditions. In this case, polymer architecture would be a dominant feature, since linear polymers are less shear-stable than branched ones [81]. Therefore, Dex/HA 0.047, which approaches full network formation, might better resist extreme shear rates than Dex/HA with slightly lower crosslinking density.

The 3ITT was shear rate based, since in the event of bioprinting one also prefers to control the shear rate (~extrusion flow) rather than the shear stress. However, this means that more viscous bioinks experienced higher shear stress during the measurement, while polymer degradation has proven to be dependent on shear stress rather than rate [82]. Therefore, the larger percentage viscosity loss for more viscous Dex/HA might at least partly be due to higher stress, instead of the aforementioned mechanisms.

Several studies have emphasized the importance of bioink yield stress, which is a minimum stress required to make the material flow [23, 27]. The presence of a yield stress implicates that once extruded, the material ceases to flow and therefore yields excellent shape fidelity. However, this might be irrelevant for pre-crosslinked Dex/HA because of its permanent viscosity loss. It is very likely that the initial yield stress is not maintained after application of stress, e.g. during extrusion. Further rheological analysis might elucidate whether the Dex/HA formulations still possess a yield stress after extrusion. Nevertheless, yield stresses were determined for Dex/HA 0.040, 0.044 and 0.047 (**Table 1**). Remarkably, a higher yield stress was found for Dex/HA 0.040 than for 0.044. Even more remarkable is that Dex/HA 0.044 would have the lowest yield stress, but also required the highest pressure to be extruded from the bioprinter (**Figure 10**). Most likely, this must be attributed to the poor reproducibility of Dex/HA pre-crosslinking. In reality, the sample of Dex/HA 0.044 used for printing might have possessed a much higher yield stress than the sample of which the yield stress was determined.

This leads to some practical considerations regarding rheological analysis. The combination of poor pre-crosslinking reproducibility and permanent viscosity loss in the pre-crosslinked material makes it quite difficult to truly determine the properties of the material that one is working with. After a rheological measurement, the initial properties will never be restored, which will impact any subsequent rheological analyses or experimental applications. For example, the viscosity values stated in **Table 1** correspond to the exact same samples as have been assessed for printability, but the viscosity at the time of printing is unknown and without a doubt lower than the viscosity that was measured initially. Dex/HA is costly material, so rheological analyses have to be designed intelligently if one can only perform a single 'true' measurement for each sample.

### 4.3 Printability

Printability assessment showed that Dex/HA 0.033 had no shape fidelity after printing and was considered not to be printable (**Figure 10**). Supported by that fact that 0.033 was extrudable at much lower pressure than the other Dex/HA bioinks, while being less shear thinning, this can be attributed to its low viscosity and presumed absence of yield stress (**Table 1**). In contrast, Dex/HA 0.040, 0.044 and 0.047 were printable for at least one set of printing parameters. Compared to Cellink Start, the minimal extrusion pressure was quite high: Cellink Start was

printable at 10 kPa, whereas up to at least 50 kPa, no continuous extrusion of Dex/HA was obtained. Higher pressure implies that bioprinted cells will experience higher shear stress, so the effect on cell viability needs to be investigated in the future.

When comparing Cellink Start and Dex/HA 0.040, the difference in extrusion pressure cannot readily be explained by the rheological parameters listed in **Table 1**. The viscosities are similar, Dex/HA 0.040 is more shear thinning, and Cellink Start has a higher yield stress, which would all suggest that Dex/HA is easier to extrude. A plausible explanation is the consistency of Dex/HA, which is visibly heterogeneous. Especially with the highest levels of crosslinking (0.044 and 0.047 H<sub>2</sub>O<sub>2</sub>/TA), the polymer solutions have a somewhat granulated appearance. This was not further quantified in this study, but one can imagine that if 'gel particles' are formed due to locally high crosslinking density, it requires more pressure to extrude these. Indeed, extrusion of Dex/HA 0.040, 0.044 and 0.047 was very inconsistent. At one moment, nothing was extruded, while the next moment, a burst of extrusion was observed. Similar findings were obtained while printing with 10% Dex/HA (Dex-TA: O/DS15) + 0.023 H<sub>2</sub>O<sub>2</sub>/TA using the BIO X printer at the Sahlgrenska Academy. The material heterogeneity also explains why the filament edges are not smooth (**Table 1**).

The effect of low viscosity recovery can be seen in the filament spread and diameter variation of the printed filaments (**Table 1**). Because of the viscosity drop which lasts after extrusion, the material can spread out. It makes sense that the extent of spreading and therefore the filament width increased with decreasing viscosity. However, the resulting filament spread values of between 1.23 and 1.96, corresponding to ~500-800 µm filament width, are acceptable, especially when similar accuracy could be demonstrated for smaller nozzle diameters.

#### **4.4 Dex/HA as a carrier for iPSC chondrogenesis and bioprinting**

Previously, optimization of chondrogenesis of iPSCs in Dex/HA has been attempted by comparing different cell densities [71] and chondrogenic medium composition [83, 84]. However, in all cases the hydrogel itself had the same composition of 10% polymer dissolved in PBS. It was hypothesized that lowering the polymer concentration of Dex/HA gels would enhance iPSC viability and chondrogenesis. Yet, ACAN-GFP expression (**Figure 13**) and histological results (**Figure 14**) show only minor differences between Dex/HA hydrogels with 2.5, 5 and 10% polymer concentration and based on polymer solutions in PBS, DMEM, Matrigel and ddH<sub>2</sub>O as potential carrier for the iPSC cell line. This is considered particularly remarkable for ddH<sub>2</sub>O, which is hypotonic compared to intracellular fluids and therefore usually induces cell lysis. Most likely, high permeability of the hydrogel allowed rapid diffusion of minerals and other components from the culture medium as soon as this was added, minimizing the harmful effects of ddH<sub>2</sub>O.

Although increase of ACAN-GFP expression is observed over the course of five weeks, histological sections suggest few or no matrix production. If new tissue had formed inside the hydrogel, the structure of the cryosections would presumably be less ruptured and have a higher integrity compared to cell-free controls, which was not the case here (**Figure S5**). It is known that for the iPS cell line, without pre-differentiation, co-culture or conditioned medium, five weeks chondrogenic culture might indeed not be sufficient for the initiation of matrix production. Apparent strong ACAN-GFP signal (**Figure 13**) has to be considered with care, because the imaging intensity settings were based on the maximal intensity value measured over all conditions. Moreover, it should be noted that the ACAN-GFP signal indicates expression on the mRNA level. Subsequent aggrecan synthesis on the protein level will have a certain delay.

In the absence of additional quantitative assessment of cell viability, activity or differentiation, no further conclusions on the optimal Dex/HA composition for iPSC chondrogenesis can be drawn. However, with a view to bioprinting, it is recommendable not to use a polymer concentration as low as 2.5%, because the gel is very soft and expected to present poor shape fidelity as a bioink. Components of culture media such as DMEM and Matrigel could reduce H<sub>2</sub>O<sub>2</sub>, interfering in the crosslinking process, whereas ddH<sub>2</sub>O might still impair cell viability when cells are present in the gel precursor for a prolonged time, which is not unlikely in the bioprinting process. Therefore, PBS appears to be the most suitable material for Dex/HA bioprinting with (iPS) cells. If for any reason the use of a cell culture medium is preferred, the formulation should be carefully selected. Medium including pyruvate, as was used here, should be avoided, since pyruvate has a high affinity to react with H<sub>2</sub>O<sub>2</sub> [85, 86].

#### **4.5 Metabolic activity of iPSCs in Dex/HA**

Common methods to assess cell viability are not suitable for cells encapsulated in Dex/HA: for cytometry in an automatic cell counter cells need to be in (single cell) suspension, whereas live/dead staining suffers from elevated background signal due to Dex/HA absorbing ethidium homodimer-1. Therefore, it was suggested to use PrestoBlue, a metabolic assay that can be used to estimate viable cell number and has been executed successfully for MSCs encapsulated in Dex/HA [47]. However, no conversion of PrestoBlue could be detected for Dex/HA-encapsulated iPSCs (**Figure S2 and S3**). It should be noted that absorbance was measured, which is less sensitive than fluorescence.

Comparing the conversion after 24 hours PrestoBlue incubation of iPSCs in suspension, pellet culture and Dex/HA culture, both 3D cultures yielded less resazurin reduction compared to the suspension. Yet, the difference between pellet en Dex/HA culture is large as well. Lower PrestoBlue conversion in 3D cultures might be caused by diffusion limitations, but this is not plausible considering the long incubation time of 24 hours. The energy production of pluripotent

cells has been found to rely on increased glycolysis and diminished oxidative phosphorylation compared to differentiated cells [87-89]. Although this does not provide a full explanation of the PrestoBlue results, it might contribute to the low levels of conversion. This implicates that caution is required when using any metabolic assay to estimate viable numbers of differentiating cells.

PrestoBlue claims to be non-cytotoxic, but it obviously has an adverse effect on iPSC pellet cultures (**Figure S4**). It seems that this has not been described in literature yet and therefore would be interesting to investigate more thoroughly. Importantly, the Dex/HA cultures used for ACAN expression and histological analysis have been exposed to 24 hour-incubation in PrestoBlue multiple times, which might have affected the iPSCs. Based on these results, it is not recommended to use PrestoBlue for longitudinal real-time measurements, but only as an end-point assay.

#### **4.6 Bioprinting of iPSC-laden Dex/HA**

The feasibility of printing iPSC-laden Dex/HA with homogeneous cell distribution was shown (**Figure 17**). However, based on histology only, it cannot be determined whether the iPSCs are still viable and functional after the printing process. Although the cell-laden Dex/HA that yielded this results was not subjected to rheological analysis, the viscosity was visibly similar as without iPSCs. In contrast, when the same concentration of iPSCs ( $10^7/\text{mL}$ ) was added to the Dex/HA used for rheological characterization and further experiments, viscosity drastically decreased (**Figure 16**). The differences between both were the Dex-TA batch, the polymer concentration (10% versus 5%) and the corresponding  $\text{H}_2\text{O}_2$  concentration (0.00375 versus 0.0030). The polymer concentration might very well be causing the difference in viscosity as response to incorporation of cells. iPSCs have a diameter of  $\sim 15 \mu\text{m}$ , whereas the polymers have a hydrodynamic radius of only several nanometres. Therefore, it takes many connected polymer molecules to enclose a cell. At lower polymer concentration, this has a lower probability to take place. Instead, 'fragments' of polymers network are formed in between the cells. Furthermore, iPSCs (as well as other cell types) might release compounds into the gel precursor that scavenge  $\text{H}_2\text{O}_2$ . Therefore, the residence time of iPSCs in the gel precursor prior to crosslinking is of importance, as well as the cell metabolism, which on its turn depends on many factors. Finally, it has been considered whether the polymer crosslinking might be disturbed by interactions between TA-groups and cell membrane-bound tyrosines, which can form on-cell crosslinks via the HRP/ $\text{H}_2\text{O}_2$  mediated crosslinking mechanism [43]. Because the  $\text{H}_2\text{O}_2$  concentration used to crosslink 5% Dex/HA was lower than for 10%, while the cell concentration was identical, this interference would have a larger effect on the crosslinking of 5% Dex/HA. However, while the typical number of on-cell crosslinks per cell is unknown, it is unlikely to be sufficiently large to significantly affect the polymer crosslinking density, in part because the affinity between TA groups is higher than between TA and tyrosine.

It is believed that for a specific cell type and cell concentration, it is possible to tune the viscosity once again by increasing the H<sub>2</sub>O<sub>2</sub> concentration. However, it is more desirable to have a bioink that does not need to be adapted for each cell type and concentration. Instead, cells might be mixed in after Dex/HA pre-crosslinking (**Figure 16**), although this complicates the achievement of homogeneous cell distribution [23].

Cell sedimentation inside viscous Dex/HA has to be taken into account in case of lower viscosities, but might not be a problem in the formulations that were found to be printable (**Figure 15**). It must be noted that also in this experiment, Dex/HA crosslinking possibly has been impaired by the presence of iPSCs. However, a ten-fold lower concentration (10<sup>6</sup> cells/mL) was used here and seemingly did not have a major effect on the viscosity.

#### **4.7 Recommendations and future outlook**

In this study, several steps were undertaken to investigate the suitability of Dex/HA for 3D bioprinting, supported by new insights in the material's rheological properties. The strategy that was chosen, which enzymatic pre-crosslinking to create a viscous bioink, seemed an elegant approach because of its simplicity. However, finding a procedure yielding reproducible bioinks appeared to be rather complicated. The inconsistent and seemingly heterogeneous pre-crosslinking proposed the main obstacle for creating a robust Dex/HA bioink. Clarification of this phenomenon would be very interesting for both fundamental understanding of the crosslinking process, as well as the application of bioprinting. In future experiments it could be determined whether increased polymer concentration and/or the use of another Dex-TA batch improves the pre-crosslinking reproducibility. It is however not unlikely that also further investigation will lead to the conclusion that pre-crosslinked Dex/HA, especially in combination with cells, is not a reproducible bioink for simple extrusion printing.

However, the results of this study can also be used as a starting point for alternative approaches. First of all, rheological analysis points out that when Dex/HA is partially crosslinked, it exhibits appropriate viscosity and shear thinning behaviour. It is therefore likely that these properties can also be obtained when Dex/HA is pre-crosslinked using another crosslinking modality. For example, the use of photo-initiators that absorb visible light have enhanced the attractiveness of photo-crosslinking, since this is much more cell-compatible than conventional UV-crosslinking [73, 90, 91]. This potentially offers a solution to achieve homogeneous pre-crosslinking. Instead of pre-crosslinking, Dex/HA solution could be supplemented with high molecular (non-functionalized) HA, nanofibrillated cellulose or another polymer that is known to increase viscosity and shear thinning.

As stated in the introduction, bioprinting techniques are developing more rapidly than bioinks, but also the two are increasingly considered as an integrated platform. For example, co-axial printing is a good example where the technique can be said to enhance the bioink. Fast cross-linking by co-axial extrusion of the crosslinking agent yields rapid shape stabilization, posing less strict rheological requirements of the bioink. Lower viscosity inks can be used, which allow homogeneous cell mixing even after pre-crosslinking. In the case of Dex/HA, this way the interference of cells with enzymatic crosslinking could be avoided. Furthermore, lower extrusion pressure if required for lower pre-printing viscosity, which decreased the shear stress on incorporated cells. Co-extrusion of Dex/HA 0.040 with H<sub>2</sub>O<sub>2</sub> solution was already attempted on the INKREDIBLE+ printer using a 26G/20G coaxial nozzle (data not shown), but the extrusion pressure resolution of 1 kPa of the printer was too low for controlled extrusion of H<sub>2</sub>O<sub>2</sub> solution. This can be solved by using other instrumentation or increasing the viscosity.

Yet another strategy is the incorporation of alginate-calcium crosslinking. In contrast to the enzymatic crosslinking process, which is delayed and permanent, ionic alginate crosslinking is an instantaneous and reversible process. Co-axial extrusion of Dex/HA with calcium (inner nozzle) and alginate with H<sub>2</sub>O<sub>2</sub> (outer nozzle) would provide an immediately crosslinked alginate shell that maintains the shape of the Dex/HA core until it is enzymatically crosslinked. Afterwards, alginate crosslinking can be reversed by EDTA incubation and the alginate can be removed from the construct. A disadvantage of this approach is that upon removal of alginate, stacked layers of 3D constructs will not be integrated.

A consideration for future experiments is the Dex/HA polymer concentration. For the purpose of bioprinting, it is recommended to use between 5% and 10% w/v polymer concentration, because lower concentration gels lack the mechanical strength required for 3D bioprinting, whereas higher concentrations result in a more tacky material and in general impair cell migration and function. For the latter reason, 5% Dex/HA was chosen over 10% in this study. However, this resulted in increased sensitivity of the pre-crosslinking process towards H<sub>2</sub>O<sub>2</sub> concentration and the incorporation of iPSCs. Therefore, it is recommended to include 10% and/or intermediate polymer concentrations in further research on Dex/HA bioprinting.

As soon as a better Dex/HA bioprinting platform has been established, it is of major importance to investigate cell survival after the printing process, mechanical properties and chondrogenic potential of printed constructs. In addition to iPSCs, it is worth investigating the potential of Dex/HA bioprinting for CTE using other cell types, such as chondrocytes and MSCs.

## 5 CONCLUSIONS

In this study, the potential of bioprinting Dex-TA/HA-TA with iPSCs was demonstrated. A variety of Dex-TA/HA-TA compositions were found to be compatible with iPSCs, but for bioprinting the composition must be restricted to 5 – 10% polymer concentration and polymer solutions in PBS. Enzymatic pre-crosslinking can be used to tune the viscosity of Dex-TA/HA-TA solutions, resulting in printable bioinks that are shear thinning, possess yield stress and present permanent viscosity loss after shear. Dex-TA/HA-TA pre-crosslinking was found to be a sensitive and heterogeneous mechanism, resulting in poor reproducibility, and was strongly impacted by the presence of iPSCs.

# ACKNOWLEDGEMENTS

Just over a year ago, I started with the first part of this master thesis project at the Sahlgrenska Academy in Gothenburg. I would like to thank everyone who contributed to the work presented in this thesis, but also to my stay in Gothenburg, which has been a very valuable experience to me.

Most of all, I want to thank my daily supervisors Stina Simonsson and Sanne Both. It was a pleasure to work under your supervision. Stina, your commitment and sharp mind have been an example, which definitely contributed to my professional development and the level of this thesis. Sanne, after returning to Enschede I sometimes struggled with getting things going again, but you always expressed your trust in me and helped me with setting clear and realistic goals.

I would like to thank Anders Lindahl and the entire Molecular Cell Biology group for their hospitality. Marieke, Carl, Camilla and Marianne, thanks for your support in and around the lab and above all for your contribution to the pleasant time that I had at Sahlgrenska.

Dr. Roland Kádár of the Chalmers University of Technology was the first to introduce me to the field of polymer rheology. I would like to express my gratitude towards him for sharing his knowledge, allowing me to perform measurements in his lab and even providing a custom-made setup. Although it did not end up in this thesis, I also would like to thank Claas Willem Visser from the Physics of Fluids Group at Twente and his student Ewout Zuiderduin for allowing me to investigate co-axial printing with the use of their materials.

I would like to express my appreciation towards the members of my graduation committee: Marcel Karperien for all the nice and useful discussions about my project; Bram Zoetebier for sharing his expertise on the hydrogel and rheology measurements; and Jeroen Rouwkema for taking the time to give his independent judgment by fulfilling the role of external member.

I am very grateful to all the members of the DBE group that helped me out at some point, even during the weekends so that I was able to take care of my cell culture. Malin Becker and Maik Schot, thank you for thinking along with me on the subjects of rheology and bioprinting. The lunch walks with my friends, coffee breaks with BME peers and chats with fellow DBE students really helped me through the tougher moments during the past months.

Finally, I want to thank my parents for supporting me throughout my studies and allowing me to seize many amazing opportunities along the way.

## REFERENCES

1. Driban, J.B., et al., *Association of knee injuries with accelerated knee osteoarthritis progression: data from the Osteoarthritis Initiative*. *Arthritis Care Res (Hoboken)*, 2014. **66**(11): p. 1673-9.
2. Muthuri, S.G., et al., *History of knee injuries and knee osteoarthritis: a meta-analysis of observational studies*. *Osteoarthritis Cartilage*, 2011. **19**(11): p. 1286-93.
3. Tarride, J.E., et al., *The excess burden of osteoarthritis in the province of Ontario, Canada*. *Arthritis Rheum*, 2012. **64**(4): p. 1153-61.
4. Lourenço, S., et al., *Osteoarthritis medical labelling and health-related quality of life in the general population*. *Health and quality of life outcomes*, 2014. **12**: p. 146-146.
5. Boutron, I., et al., *Disability and quality of life of patients with knee or hip osteoarthritis in the primary care setting and factors associated with general practitioners' indication for prosthetic replacement within 1 year*. *Osteoarthritis Cartilage*, 2008. **16**(9): p. 1024-31.
6. McAlindon, T.E., et al., *OARSI guidelines for the non-surgical management of knee osteoarthritis*. *Osteoarthritis Cartilage*, 2014. **22**(3): p. 363-88.
7. Bayliss, L.E., et al., *The effect of patient age at intervention on risk of implant revision after total replacement of the hip or knee: a population-based cohort study*. *The Lancet*, 2017. **389**(10077): p. 1424-1430.
8. Guermazi, A., et al., *Brief Report: Partial- and Full-Thickness Focal Cartilage Defects Contribute Equally to Development of New Cartilage Damage in Knee Osteoarthritis: The Multicenter Osteoarthritis Study*. *Arthritis Rheumatol*, 2017. **69**(3): p. 560-564.
9. Everhart, J.S., M.M. Abouljoud, and D.C. Flanigan, *Role of full-thickness cartilage defects in knee osteoarthritis (OA) incidence and progression: Data from the OA Initiative*. *J Orthop Res*, 2019. **37**(1): p. 77-83.
10. Wluka, A.E., et al., *The clinical correlates of articular cartilage defects in symptomatic knee osteoarthritis: a prospective study*. *Rheumatology (Oxford)*, 2005. **44**(10): p. 1311-6.
11. Steadman, J.R., et al., *Microfracture technique for full-thickness chondral defects: Technique and clinical results*. *Operative Techniques in Orthopaedics*, 1997. **7**(4): p. 300-304.
12. Kreuz, P.C., et al., *Results after microfracture of full-thickness chondral defects in different compartments in the knee*. *Osteoarthritis Cartilage*, 2006. **14**(11): p. 1119-25.
13. Brittberg, M., et al., *Treatment of deep cartilage defects in the knee with autologous chondrocyte transplantation*. *N Engl J Med*, 1994. **331**(14): p. 889-95.
14. DiBartola, A.C., et al., *Correlation between histological outcome and surgical cartilage repair technique in the knee: A meta-analysis*. *Knee*, 2016. **23**(3): p. 344-9.
15. Kon, E., et al., *Scaffold-based cartilage treatments: with or without cells? A systematic review of preclinical and clinical evidence*. *Arthroscopy*, 2015. **31**(4): p. 767-75.
16. Schrock, J.B., et al., *A Cost-Effectiveness Analysis of Surgical Treatment Modalities for Chondral Lesions of the Knee: Microfracture, Osteochondral Autograft Transplantation, and Autologous Chondrocyte Implantation*. *Orthop J Sports Med*, 2017. **5**(5): p. 2325967117704634.
17. Everhart, J.S., et al., *Cost-efficacy of Knee Cartilage Defect Treatments in the United States*. *Am J Sports Med*, 2019: p. 363546519834557.
18. Aae, T.F., et al., *Microfracture is more cost-effective than autologous chondrocyte implantation: a review of level 1 and level 2 studies with 5 year follow-up*. *Knee Surg Sports Traumatol Arthrosc*, 2018. **26**(4): p. 1044-1052.
19. Stein, S., E. Strauss, and J. Bosco, 3rd, *Advances in the Surgical Management of Articular Cartilage Defects: Autologous Chondrocyte Implantation Techniques in the Pipeline*. *Cartilage*, 2013. **4**(1): p. 12-9.

20. Gao, T., et al., *Optimization of gelatin-alginate composite bioink printability using rheological parameters: a systematic approach*. *Biofabrication*, 2018. **10**(3): p. 034106.
21. Holzl, K., et al., *Bioink properties before, during and after 3D bioprinting*. *Biofabrication*, 2016. **8**(3): p. 032002.
22. Li, H., S. Liu, and L. Lin, *Rheological study on 3D printability of alginate hydrogel and effect of graphene oxide*. *International Journal of Bioprinting*, 2016. **2**(2).
23. Mouser, V.H., et al., *Yield stress determines bioprintability of hydrogels based on gelatin-methacryloyl and gellan gum for cartilage bioprinting*. *Biofabrication*, 2016. **8**(3): p. 035003.
24. Ouyang, L., et al., *Effect of bioink properties on printability and cell viability for 3D bioplotting of embryonic stem cells*. *Biofabrication*, 2016. **8**(3): p. 035020.
25. Paxton, N., et al., *Proposal to assess printability of bioinks for extrusion-based bioprinting and evaluation of rheological properties governing bioprintability*. *Biofabrication*, 2017. **9**(4): p. 044107.
26. Ribeiro, A., et al., *Assessing bioink shape fidelity to aid material development in 3D bioprinting*. *Biofabrication*, 2017. **10**(1): p. 014102.
27. Kiyotake, E.A., et al., *Development and quantitative characterization of the precursor rheology of hyaluronic acid hydrogels for bioprinting*. *Acta Biomater*, 2019. **95**: p. 176-187.
28. Daly, A.C., et al., *A comparison of different bioinks for 3D bioprinting of fibrocartilage and hyaline cartilage*. *Biofabrication*, 2016. **8**(4): p. 045002.
29. Izadifar, Z., et al., *Analyzing Biological Performance of 3D-Printed, Cell-Impregnated Hybrid Constructs for Cartilage Tissue Engineering*. *Tissue Eng Part C Methods*, 2016. **22**(3): p. 173-88.
30. Kundu, J., et al., *An additive manufacturing-based PCL-alginate-chondrocyte bioprinted scaffold for cartilage tissue engineering*. *Journal of Tissue Engineering and Regenerative Medicine*, 2015. **9**(11): p. 1286-1297.
31. Yang, X., et al., *Collagen-alginate as bioink for three-dimensional (3D) cell printing based cartilage tissue engineering*. *Mater Sci Eng C Mater Biol Appl*, 2018. **83**: p. 195-201.
32. Markstedt, K., et al., *3D Bioprinting Human Chondrocytes with Nanocellulose-Alginate Bioink for Cartilage Tissue Engineering Applications*. *Biomacromolecules*, 2015. **16**(5): p. 1489-96.
33. Nguyen, D., et al., *Cartilage Tissue Engineering by the 3D Bioprinting of iPS Cells in a Nanocellulose/Alginate Bioink*. *Sci Rep*, 2017. **7**(1): p. 658.
34. Costantini, M., et al., *3D bioprinting of BM-MSCs-loaded ECM biomimetic hydrogels for in vitro neocartilage formation*. *Biofabrication*, 2016. **8**(3): p. 035002.
35. Idaszek, J., et al., *3D bioprinting of hydrogel constructs with cell and material gradients for the regeneration of full-thickness chondral defect using a microfluidic printing head*. *Biofabrication*, 2019. **11**(4): p. 044101.
36. Noble, P.W., *Hyaluronan and its catabolic products in tissue injury and repair*. *Matrix Biology*, 2002. **21**(1): p. 25-29.
37. Mouser, V.H., et al., *Development of a thermosensitive HAMA-containing bio-ink for the fabrication of composite cartilage repair constructs*. *Biofabrication*, 2017. **9**(1): p. 015026.
38. Pati, F., et al., *Printing three-dimensional tissue analogues with decellularized extracellular matrix bioink*. *Nat Commun*, 2014. **5**: p. 3935.
39. Kesti, M., et al., *Bioprinting Complex Cartilaginous Structures with Clinically Compliant Biomaterials*. *Advanced Functional Materials*, 2015. **25**(48): p. 7406-7417.
40. Jin, R., et al., *Enzyme-mediated fast in situ formation of hydrogels from dextran-tyramine conjugates*. *Biomaterials*, 2007. **28**(18): p. 2791-800.
41. Moreira Teixeira, L.S., et al., *Self-attaching and cell-attracting in-situ forming dextran-tyramine conjugates hydrogels for arthroscopic cartilage repair*. *Biomaterials*, 2012. **33**(11): p. 3164-74.

42. Wennink, J.W.H., et al., *Injectable Hydrogels by Enzymatic Co-Crosslinking of Dextran and Hyaluronic Acid Tyramine Conjugates*. Macromolecular Symposia, 2011. **309-310**(1): p. 213-221.
43. Kamperman, T., et al., *Direct on-cell crosslinked hydrogel microniches with on-demand tunable stiffness to program single stem cell fate*, in *Microgel technology to advance modular tissue engineering (PhD thesis)*. 2018, University of Twente: Enschede, The Netherlands. p. 53-71.
44. Kamperman, T., et al., *Centering Single Cells in Microgels via Delayed Crosslinking Supports Long-Term 3D Culture by Preventing Cell Escape*. Small, 2017. **13**(22): p. 1603711.
45. Moreira Teixeira, L.S., et al., *High throughput generated micro-aggregates of chondrocytes stimulate cartilage formation in vitro and in vivo*. European Cells and Materials, 2012. **23**: p. 387-399.
46. Portalska, K.J., et al., *Boosting Angiogenesis and Functional Vascularization in Injectable Dextran–Hyaluronic Acid Hydrogels by Endothelial-Like Mesenchymal Stromal Cells*. Tissue Engineering Part A, 2013. **20**(3-4): p. 819-829.
47. Henke, S., et al., *Enzymatic Crosslinking of Polymer Conjugates is Superior over Ionic or UV Crosslinking for the On-Chip Production of Cell-Laden Microgels*. Macromol Biosci, 2016. **16**(10): p. 1524-1532.
48. Russell, K.C., et al., *In Vitro High-Capacity Assay to Quantify the Clonal Heterogeneity in Trilineage Potential of Mesenchymal Stem Cells Reveals a Complex Hierarchy of Lineage Commitment*. STEM CELLS, 2010. **28**(4): p. 788-798.
49. Peltari, K., et al., *Premature induction of hypertrophy during in vitro chondrogenesis of human mesenchymal stem cells correlates with calcification and vascular invasion after ectopic transplantation in SCID mice*. Arthritis Rheum, 2006. **54**(10): p. 3254-66.
50. Janicki, P., et al., *Chondrogenic pre-induction of human mesenchymal stem cells on beta-TCP: enhanced bone quality by endochondral heterotopic bone formation*. Acta Biomater, 2010. **6**(8): p. 3292-301.
51. Stenderup, K., et al., *Aging is associated with decreased maximal life span and accelerated senescence of bone marrow stromal cells*. Bone, 2003. **33**(6): p. 919-26.
52. Bonab, M.M., et al., *Aging of mesenchymal stem cell in vitro*. BMC cell biology, 2006. **7**: p. 14-14.
53. Takahashi, K., et al., *Induction of Pluripotent Stem Cells from Adult Human Fibroblasts by Defined Factors*. Cell, 2007. **131**(5): p. 861-872.
54. Fujihara, Y., T. Takato, and K. Hoshi, *Immunological response to tissue-engineered cartilage derived from auricular chondrocytes and a PLLA scaffold in transgenic mice*. Biomaterials, 2010. **31**(6): p. 1227-1234.
55. Smith, B., I.R. Sigal, and D.A. Grande, *Immunology and cartilage regeneration*. Immunologic Research, 2015. **63**(1): p. 181-186.
56. Kim, K., et al., *Epigenetic memory in induced pluripotent stem cells*. Nature, 2010. **467**(7313): p. 285-90.
57. Polo, J.M., et al., *Cell type of origin influences the molecular and functional properties of mouse induced pluripotent stem cells*. Nat Biotechnol, 2010. **28**(8): p. 848-55.
58. Bar-Nur, O., et al., *Epigenetic memory and preferential lineage-specific differentiation in induced pluripotent stem cells derived from human pancreatic islet beta cells*. Cell Stem Cell, 2011. **9**(1): p. 17-23.
59. Borestrom, C., et al., *Footprint-free human induced pluripotent stem cells from articular cartilage with redifferentiation capacity: a first step toward a clinical-grade cell source*. Stem Cells Transl Med, 2014. **3**(4): p. 433-47.
60. Yamashita, A., et al., *Generation of scaffoldless hyaline cartilaginous tissue from human iPSCs*. Stem Cell Reports, 2015. **4**(3): p. 404-18.
61. Suchorska, W.M., et al., *Comparison of Four Protocols to Generate Chondrocyte-Like Cells from Human Induced Pluripotent Stem Cells (hiPSCs)*. Stem Cell Rev, 2017. **13**(2): p. 299-308.

62. Nejadnik, H., et al., *Improved approach for chondrogenic differentiation of human induced pluripotent stem cells*. Stem Cell Rev, 2015. **11**(2): p. 242-53.
63. Medvedev, S.P., et al., *Human induced pluripotent stem cells derived from fetal neural stem cells successfully undergo directed differentiation into cartilage*. Stem Cells Dev, 2011. **20**(6): p. 1099-112.
64. Ko, J.Y., et al., *In vitro chondrogenesis and in vivo repair of osteochondral defect with human induced pluripotent stem cells*. Biomaterials, 2014. **35**(11): p. 3571-81.
65. Guzzo, R.M., et al., *Efficient differentiation of human iPSC-derived mesenchymal stem cells to chondroprogenitor cells*. J Cell Biochem, 2013. **114**(2): p. 480-90.
66. Craft, A.M., et al., *Generation of articular chondrocytes from human pluripotent stem cells*. Nat Biotechnol, 2015. **33**(6): p. 638-45.
67. Wei, Y., et al., *Chondrogenic differentiation of induced pluripotent stem cells from osteoarthritic chondrocytes in alginate matrix*. European Cells and Materials, 2012. **23**: p. 1-12.
68. Qu, C., et al., *Chondrogenic differentiation of human pluripotent stem cells in chondrocyte co-culture*. Int J Biochem Cell Biol, 2013. **45**(8): p. 1802-12.
69. Diekman, B.O., et al., *Cartilage tissue engineering using differentiated and purified induced pluripotent stem cells*. Proceedings of the National Academy of Sciences, 2012. **109**(47): p. 19172.
70. Liu, J., et al., *The effect of 3D nanofibrous scaffolds on the chondrogenesis of induced pluripotent stem cells and their application in restoration of cartilage defects*. PLoS One, 2014. **9**(11): p. e111566.
71. Hartl, L., *Human iPSC cells combined with a cartilage-adherent hydrogel for cartilage-like tissue engineering. (Master thesis)*. 2017, University of Twente: The Netherlands.
72. Tabriz, A.G., et al., *Three-dimensional bioprinting of complex cell laden alginate hydrogel structures*. Biofabrication, 2015. **7**(4): p. 045012.
73. Petta, D., et al., *Three-Dimensional Printing of a Tyramine Hyaluronan Derivative with Double Gelation Mechanism for Independent Tuning of Shear Thinning and Postprinting Curing*. ACS Biomaterials Science & Engineering, 2018. **4**(8): p. 3088-3098.
74. Wang, R., et al., *Cartilage adhesive and mechanical properties of enzymatically crosslinked polysaccharide tyramine conjugate hydrogels*. Polymers for Advanced Technologies, 2014. **25**(5): p. 568-574.
75. Dinkgreve, M., et al., *On different ways of measuring "the" yield stress*. Journal of Non-Newtonian Fluid Mechanics, 2016. **238**: p. 233-241.
76. Blaeser, A., et al., *Controlling Shear Stress in 3D Bioprinting is a Key Factor to Balance Printing Resolution and Stem Cell Integrity*. Adv Healthc Mater, 2016. **5**(3): p. 326-33.
77. Huang, Q., et al., *Inactivation of Horseradish Peroxidase by Phenoxy Radical Attack*. Journal of the American Chemical Society, 2005. **127**(5): p. 1431-1437.
78. Mao, L., et al., *Horseradish peroxidase inactivation: heme destruction and influence of polyethylene glycol*. Sci Rep, 2013. **3**: p. 3126.
79. Arnao, M.B., et al., *Inactivation of peroxidase by hydrogen peroxide and its protection by a reductant agent*. Biochim Biophys Acta, 1990. **1038**(1): p. 85-9.
80. Knight, J., *Mechanical Shear Degradation of Polymers in Solution: A Review*. 1976, ROYAL AIRCRAFT ESTABLISHMENT FARNBOROUGH (ENGLAND).
81. Covitch, M.J., *How Polymer Architecture Affects Permanent Viscosity Loss of Multigrade Lubricants*. 1998, SAE International.
82. Marx, N., et al., *Study of Permanent Shear Thinning of VM Polymer Solutions*. Tribology Letters, 2017. **65**(3).
83. van Dorenvanck, K., *The influence of different three dimensional culture methods and culture media on chondrocytes and induced pluripotent stem cells. (Internship report)*. 2018, University of Twente: The Netherlands.
84. Meteling, M., *The effect of Dex-HA hydrogel on the chondrogenic differentiation of encapsulated iPSC cells and chondrocytes. (Internship report)*. 2019, University of Twente: The Netherlands.

85. Babich, H., et al., *Choice of DMEM, formulated with or without pyruvate, plays an important role in assessing the in vitro cytotoxicity of oxidants and prooxidant nutraceuticals*. *In Vitro Cell Dev Biol Anim*, 2009. **45**(5-6): p. 226-33.
86. Kladna, A., et al., *Reactivity of pyruvic acid and its derivatives towards reactive oxygen species*. *Luminescence*, 2015. **30**(7): p. 1153-8.
87. Hu, L., E. Trope, and Q.-L. Ying, *Metabolism of pluripotent stem cells*. *Frontiers in Biology*, 2016. **11**(5): p. 355-365.
88. Ito, K. and K. Ito, *Metabolism and the Control of Cell Fate Decisions and Stem Cell Renewal*. *Annual Review of Cell and Developmental Biology*, 2016. **32**(1): p. 399-409.
89. Magalhaes-Novais, S., et al., *Cell quality control mechanisms maintain stemness and differentiation potential of P19 embryonic carcinoma cells*. *Autophagy*, 2019: p. 1-21.
90. Lim, K.S., et al., *Visible Light Cross-Linking of Gelatin Hydrogels Offers an Enhanced Cell Microenvironment with Improved Light Penetration Depth*. *Macromol Biosci*, 2019. **19**(6): p. e1900098.
91. Loebel, C., et al., *Microfabrication of Photo-Cross-Linked Hyaluronan Hydrogels by Single- and Two-Photon Tyramine Oxidation*. *Biomacromolecules*, 2015. **16**(9): p. 2624-2630.

# APPENDIX 1: SUPPLEMENTARY DATA

**Table S1:** Polymer batch information and overview of their application in this thesis.

Dex-TA \ HA-TA	HA-TA DS10 H18013	HA-TA DS10 H18019	HA-TA DS10 H18022
Dex-TA O/DS11 H18006	-	Figure 4	-
Dex-TA O/DS15 H18007	-	Figure 3, 4, 12, 13, 14, 17	-
Dex-TA O/DS13 H18008	Figure 4	-	-
Dex-TA N/DS12 Piet30	Figure 4	-	Figure 5, 6, 7, 8, 9, 10, 11, 15, 16; Table 1, 2
Dex-TA N/DS15 4.3	Figure 4	-	-
Dex-TA N/DS16 4.4	Figure 4	-	-

O = old synthesis method Dex-TA; N = new synthesis method Dex-TA; DS = degree of tyramine substitution; *code* = batch code as used within research group. The table indicates which combinations of Dex-TA and HA-TA have been used and which figures present results of each combination.

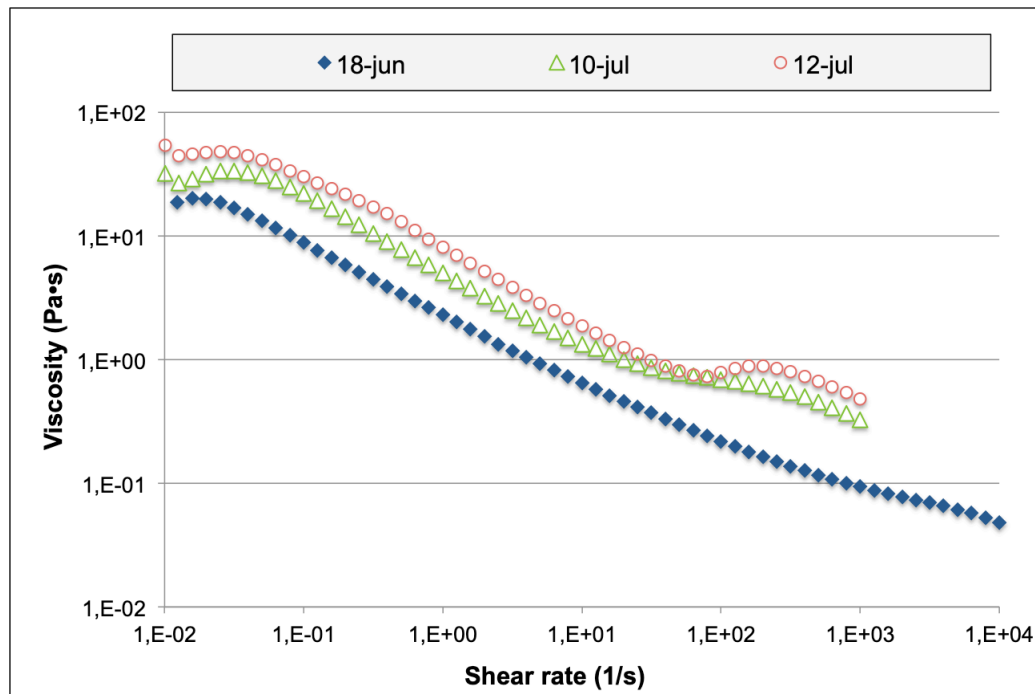


**Figure S1:** Final shear sweep viscosity measurements of Dex/HA 0.040 prepared and measured at three different dates, as indicated in the legend. Note that by accident, two of them were only measured up to a shear of 1000/s. The samples exhibit differences in viscosity, as well as in behaviour at shear rate of around 100/s. These samples were later used for bioprinting, presented in **Table 2** and **Figure 11**.

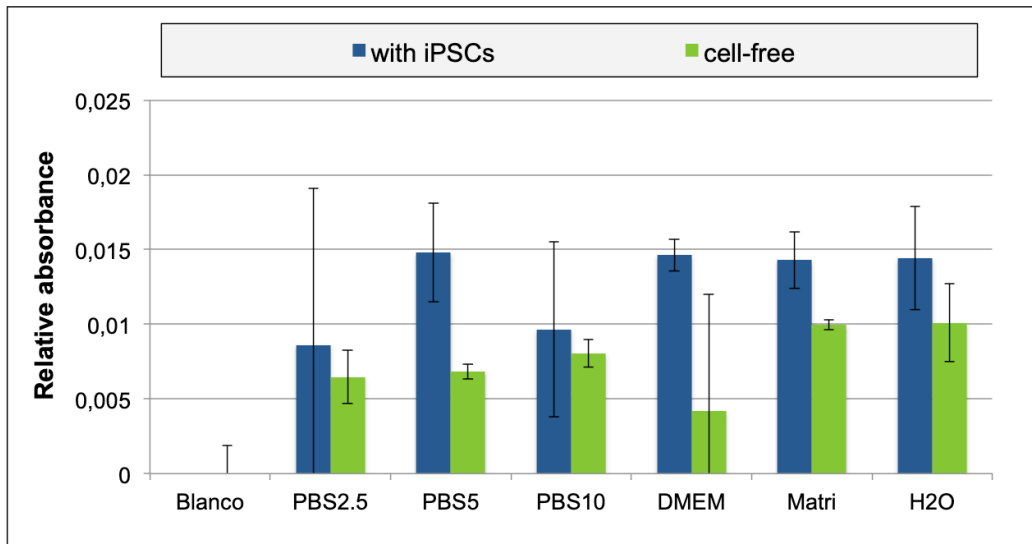


**Figure S2:** Relative absorbance representing PrestoBlue reduction of Dex/HA cultures after 21 days of chondrogenic culture. Incubation time of PrestoBlue (1:50 dilution) was 24 hours. Although for each gel composition higher absorbance is measured in presence of iPSCs compared to cell-free controls, no significant differences were found. Also note the low absorbance values, e.g. compared to **Figure S3**.

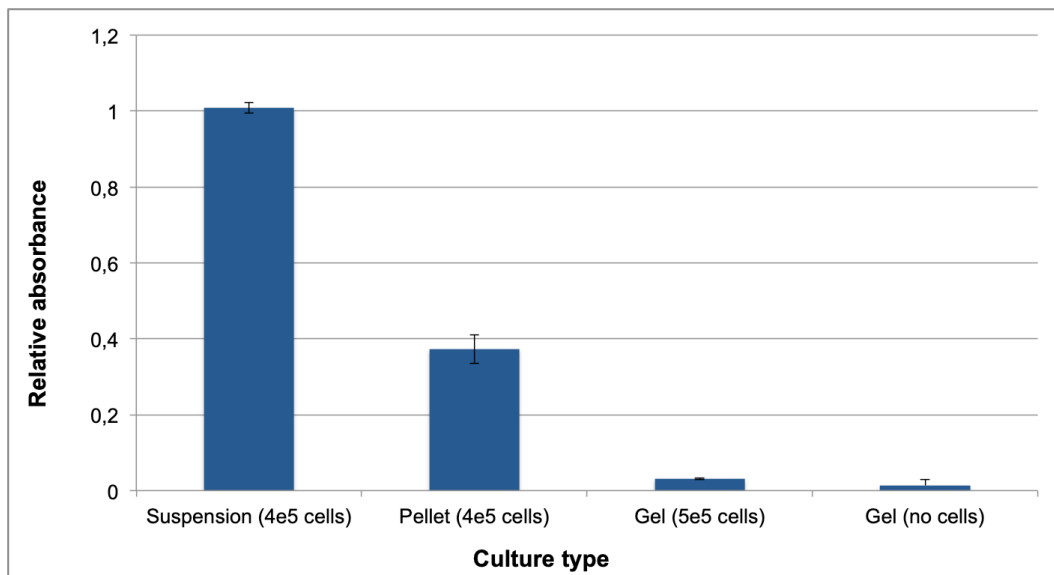


**Figure S3:** Relative absorbance representing PrestoBlue reduction by iPSCs in chondrogenic medium after 24 hours incubation in PrestoBlue (1:10 dilution).

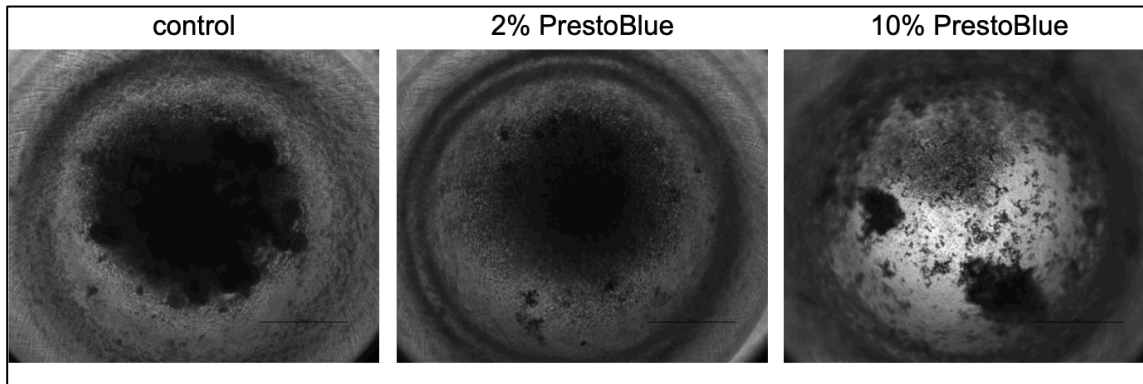


**Figure S4:** Representative images of iPSC pellets ( $2 \cdot 10^5$  cells) cultured for six days in chondrogenic medium supplemented with 0 (control), 2 or 10% PrestoBlue, the latter being the standard concentration for PrestoBlue assay. 2% PrestoBlue in the medium resulted in less dense cell pellets compared to control, whereas pellets were completely disintegrated in presence of 10% PrestoBlue.  $n=3$  for each condition. Scale bars: 1000  $\mu\text{m}$ .

**Table S2:** Gelation of 10% Dex/HA in the presence of DMEM compared to PBS. At standard  $\text{H}_2\text{O}_2$  concentration (0.03%) to obtain a solid gel, presence of DMEM delayed the gelation. At 0.00375%  $\text{H}_2\text{O}_2$ , presence of DMEM resulted in an obvious decrease of viscosity compared to PBS.

		<b>PBS</b>	<b>DMEM</b>
<b>0.03% <math>\text{H}_2\text{O}_2</math></b>	<b>Appearance</b>	Solid gel	Solid gel
	<b>Gelation time (s)</b>	$40 \pm 3$ (n=2)	$77 \pm 2$ (n=2)
<b>0.00375% <math>\text{H}_2\text{O}_2</math></b>	<b>Appearance</b>	Very viscous	Medium viscous
	<b>Gelation time (s)</b>	22s (n=1)	none (n=2)

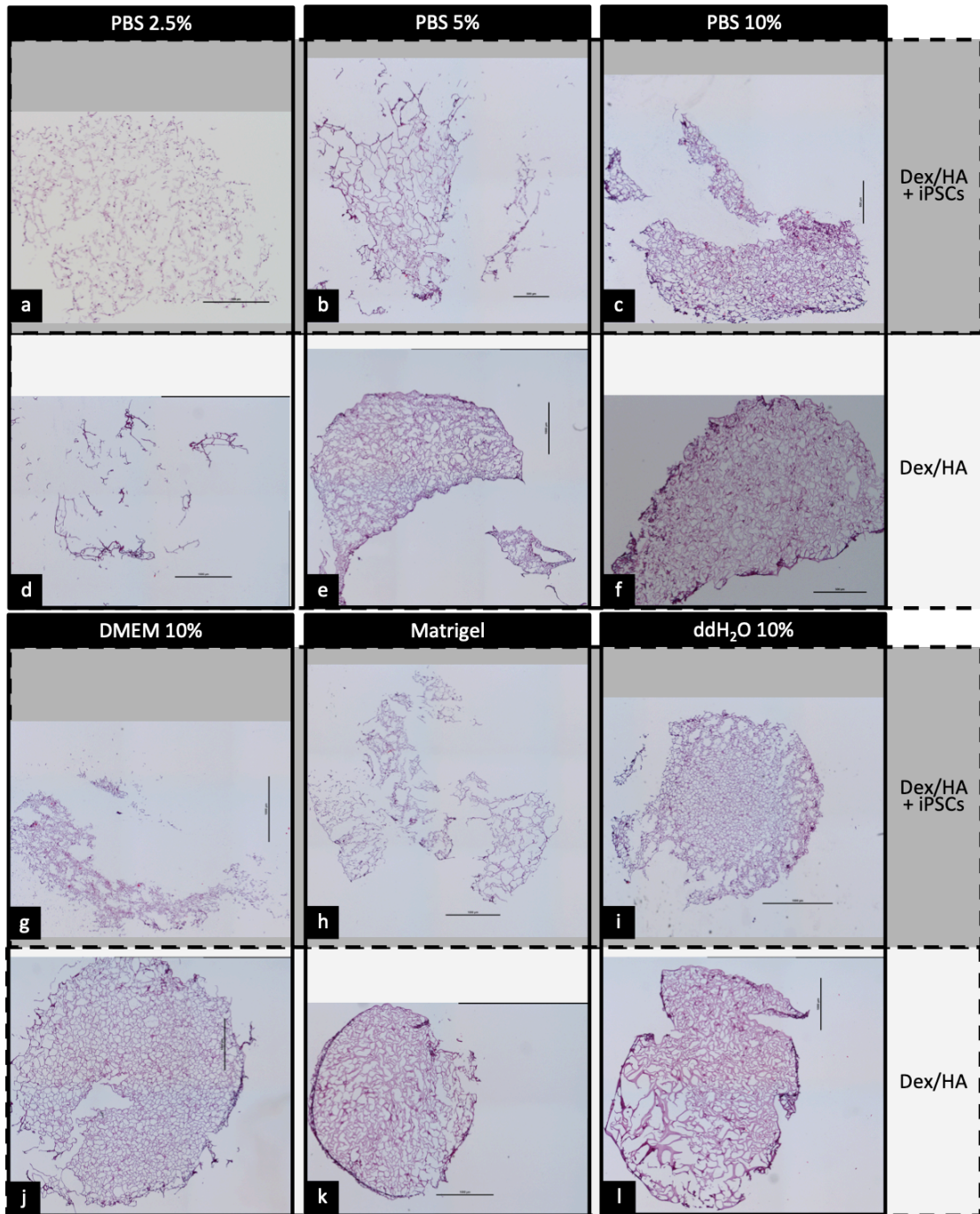


**Figure S5:** H&E-stained full sections of Dex/HA gels with (a-c and g-i) and without (d-f and j-l) iPSCs. Scale bars a-c: 500  $\mu$ m, d-l: 1000  $\mu$ m.

# APPENDIX 2: PRINTABILITY ASSESSMENT G-CODE

```
G21 ; set units to millimeters
G90 ; use absolute coordinates
M83 ; use relative distances for extrusion
G1 Z0.200 F600.000 ; move to next layer (0)
M761
G1 E-2.00000 F600.00000 ; retract extruder 0
; First extrusion pressure
G1 X22.000 Y11.939 F600.000 ; move to first perimeter point
M760
G1 E2.00000 F600.00000 ; unretract extruder 0
G1 F150 ; 1A First speed
G1 X22.000 Y22.061 E0.04499 ; perimeter
M761
G1 E-2.00000 F600.00000 ; retract extruder 0
G1 X17.000 Y11.939 F600.000 ; move to first perimeter point
M760
G1 E2.00000 F600.00000 ; unretract extruder 0
G1 F150
G1 X17.000 Y22.061 E0.04499 ; perimeter
M761
G1 E-2.00000 F600.00000 ; retract extruder 0
G1 X12.000 Y11.939 F600.000 ; move to first perimeter point
M760
G1 E2.00000 F600.00000 ; unretract extruder 0
G1 F150
G1 X12.000 Y22.061 E0.04499 ; perimeter
M761
G1 E-2.00000 F600.00000 ; retract extruder 0
G1 X5.000 Y11.939 F600.000 ; move to first perimeter point
M760
G1 E2.00000 F600.00000 ; unretract extruder 0
G1 F600 ; 1B Second speed
G1 X5.000 Y22.061 E0.04499 ; perimeter
M761
G1 E-2.00000 F600.00000 ; retract extruder 0
G1 X0.000 Y11.939 F600.000 ; move to first perimeter point
M760
G1 E2.00000 F600.00000 ; unretract extruder 0
G1 F600
G1 X-0.000 Y22.061 E0.04499 ; perimeter
M761
G1 E-2.00000 F600.00000 ; retract extruder 0
G1 X-5.000 Y11.939 F600.000 ; move to first perimeter point
M760
G1 E2.00000 F600.00000 ; unretract extruder 0
G1 F600
G1 X-5.000 Y22.061 E0.04499 ; perimeter
M761
G1 E-2.00000 F600.00000 ; retract extruder 0
G1 X-12.000 Y11.939 F600.000 ; move to first perimeter point
M760
G1 E2.00000 F600.00000 ; unretract extruder 0
G1 F1500 ; 1C Third speed
G1 X-12.000 Y22.061 E0.04499 ; perimeter
M761
G1 E-2.00000 F600.00000 ; retract extruder 0
G1 X-17.000 Y11.939 F600.000 ; move to first perimeter point
M760
G1 E2.00000 F600.00000 ; unretract extruder 0
G1 F1500
G1 X-17.000 Y22.061 E0.04499 ; perimeter
M761
G1 E-2.00000 F600.00000 ; retract extruder 0
G4 S20 ; WAIT for 20 seconds to set second extrusion pressure
G1 X-22.000 Y11.939 F600.000 ; move to first perimeter point
M760
G1 E2.00000 F600.00000 ; unretract extruder 0
G1 F1500
G1 X-22.000 Y22.061 E0.04499 ; perimeter
M761
G1 E-2.00000 F600.00000 ; retract extruder 0
G4 S20 ; WAIT for 20 seconds to set third extrusion pressure
G1 X-22.000 Y-5.061 F600.000 ; move to first perimeter point
M760
G1 E2.00000 F600.00000 ; unretract extruder 0
G1 F1500 ; 2C Third speed
G1 X-22.000 Y5.061 E0.04499 ; perimeter
M761
G1 E-2.00000 F600.00000 ; retract extruder 0
G1 X-17.000 Y-5.061 F600.000 ; move to first perimeter point
M760
G1 E2.00000 F600.00000 ; unretract extruder 0
G1 F1500
G1 X-17.000 Y5.061 E0.04499 ; perimeter
M761
G1 E-2.00000 F600.00000 ; retract extruder 0
G1 X-12.000 Y-5.061 F600.000 ; move to first perimeter point
M760
G1 E2.00000 F600.00000 ; unretract extruder 0
G1 F1500
G1 X-12.000 Y5.061 E0.04499 ; perimeter
M761
G1 E-2.00000 F600.00000 ; retract extruder 0
G1 X-5.000 Y-5.061 F600.000 ; move to first perimeter point
M760
G1 E2.00000 F600.00000 ; unretract extruder 0
G1 F600 ; 2B Second speed
G1 X-5.000 Y5.061 E0.04499 ; perimeter
M761
G1 E-2.00000 F600.00000 ; retract extruder 0
G1 X0.000 Y-5.061 F600.000 ; move to first perimeter point
M760
G1 E2.00000 F600.00000 ; unretract extruder 0
G1 F600
G1 X-0.000 Y5.061 E0.04499 ; perimeter
M761
G1 E-2.00000 F600.00000 ; retract extruder 0
G1 X5.000 Y-5.061 F600.000 ; move to first perimeter point
M760
G1 E2.00000 F600.00000 ; unretract extruder 0
G1 F600
G1 X5.000 Y5.061 E0.04499 ; perimeter
M761
G1 E-2.00000 F600.00000 ; retract extruder 0
G1 X12.000 Y-5.061 F600.000 ; move to first perimeter point
M760
G1 E2.00000 F600.00000 ; unretract extruder 0
G1 F1500 ; 2A First speed
G1 X12.000 Y5.061 E0.04499 ; perimeter
M761
G1 E-2.00000 F600.00000 ; retract extruder 0
G1 X17.000 Y-5.061 F600.000 ; move to first perimeter point
M760
G1 E2.00000 F600.00000 ; unretract extruder 0
G1 F150
G1 X17.000 Y5.061 E0.04499 ; perimeter
M761
G1 E-2.00000 F600.00000 ; retract extruder 0
G1 X22.000 Y-5.061 F600.000 ; move to first perimeter point
M760
G1 E2.00000 F600.00000 ; unretract extruder 0
G1 F150
G1 X22.000 Y5.061 E0.04499 ; perimeter
M761
G1 E-2.00000 F600.00000 ; retract extruder 0
G1 X17.000 Y-11.939 F600.000 ; move to first perimeter point
M760
```

G1 E2.00000 F600.00000 ; unretract extruder 0  
G1 F150  
G1 X16.999 Y-22.061 E0.04498 ; perimeter  
M761  
G1 E-2.00000 F600.00000 ; retract extruder 0  
G1 X12.000 Y-11.939 F600.000 ; move to first perimeter point  
M760  
G1 E2.00000 F600.00000 ; unretract extruder 0  
G1 F150  
G1 X11.999 Y-22.061 E0.04498 ; perimeter  
M761  
G1 E-2.00000 F600.00000 ; retract extruder 0  
G1 X5.000 Y-11.939 F600.000 ; move to first perimeter point  
M760  
G1 E2.00000 F600.00000 ; unretract extruder 0  
G1 F600; 3B Second speed  
G1 X4.999 Y-22.061 E0.04499 ; perimeter  
M761  
G1 E-2.00000 F600.00000 ; retract extruder 0  
G1 X-0.000 Y-11.939 F600.000 ; move to first perimeter point  
M760  
G1 E2.00000 F600.00000 ; unretract extruder 0  
G1 F600  
G1 X-0.001 Y-22.061 E0.04499 ; perimeter  
M761  
G1 E-2.00000 F600.00000 ; retract extruder 0  
G1 X-5.000 Y-11.939 F600.000 ; move to first perimeter point  
M760  
G1 E2.00000 F600.00000 ; unretract extruder 0  
G1 F600  
G1 X-5.001 Y-22.061 E0.04499 ; perimeter  
M761  
G1 E-2.00000 F600.00000 ; retract extruder 0  
G1 X-12.000 Y-11.939 F600.000 ; move to first perimeter point  
M760  
G1 E2.00000 F600.00000 ; unretract extruder 0  
G1 F1500; 3C Third speed  
G1 X-12.001 Y-22.061 E0.04498 ; perimeter  
M761  
G1 E-2.00000 F600.00000 ; retract extruder 0  
G1 X-17.000 Y-11.939 F600.000 ; move to first perimeter point  
M760  
G1 E2.00000 F600.00000 ; unretract extruder 0  
G1 F1500  
G1 X-17.001 Y-22.061 E0.04498 ; perimeter  
M761  
G1 E-2.00000 F600.00000 ; retract extruder 0  
G1 X-22.000 Y-11.939 F600.000 ; move to first perimeter point  
M760  
G1 E2.00000 F600.00000 ; unretract extruder 0  
G1 F1500  
G1 X-22.001 Y-22.061 E0.04498 ; perimeter  
M761  
G1 E-2.00000 F600.00000 ; retract extruder 0  
G1 Z45.000